University of Bath

Tailoring the electrical and thermal conductivity of multi-component and multi-phase polymer composites

Yao Huang[a,b] , Christopher Ellingford[a], Chris Bowen[c], Tony McNally[a], Daming Wu[b], Chaoying Wan[a],*

[a] *International Institute for Nanocomposites Manufacturing (IINM), WMG, University of Warwick, CV4 7AL, UK;*

[b] *Engineering Research Center for Polymer Processing Equipment, Ministry of Education, Beijing University of Chemical Technology, Beijing, China, 100029;*

[c] *Materials and Structures Centre, Department of Mechanical Engineering, University of Bath, BA2 7AY, UK*

*Corresponding author: C Wan, chaoying.wan@warwick.ac.uk

Abstract

The majority of polymers are electrical and thermal insulators, with an electrical conductivity in the range of $10^{-14} \sim 10^{-18}$ S/cm, and thermal conductivity of 0.1~0.4 W/mK. In order to create electrically active and thermally conductive polymers and composites, a number of strategies have been investigated. The current state of the art technology is to apply hybrid filler systems in polymers, i.e., to combine different types of fillers with different dimensions, in order to facilitate the formation of interconnected conducting network and to enhance the electrical, thermal, mechanical, and processing properties synergistically. The dispersion and interfacial interaction between fillers and polymers determine the final properties of polymer composites. By tailoring polymer-filler interactions both thermodynamically and kinetically, the selective localisation of fillers in polymer blends can enhance the electrical conductivity at a low percolation threshold. The percolation threshold can be further reduced by selectively dispersing fillers at the interface of co-continuous polymer blends. Moreover, the selective localisation of different types of fillers in different co-continuous phases can result in multiple functionalities, such as high electrical conductivity, thermal conductivity or electromagnetic interference shielding. In this review, we have discussed the latest progresses towards the development of electrically

1   active and thermal conductive polymer composites, and highlight the technical

2   challenges and future research directions.

3   Keywords: Electrical conductivity; Thermal conductivity; Percolation threshold;

4   Polymer composites; Phase morphology; Co-continuous morphology; Interface

5 **Introduction**

6 Polymers continue to play an increasingly important role in modern technologies due to their

7 low cost, low density, ease of manufacture and tailorable mechanical, electrical and thermal

8 properties, which have demonstrated significant potential in replacing metals and ceramics in

9 a number of applications, such as in electronics, structural engineering and automotive

10 industries. However, the electrically and thermally insulating nature of most polymers have

11 limited their engineering applications. Intrinsically electrical-conducting polymers such as

12 polyacetylene, poly(phenylene vinylene), polyaniline and polypyrrole are constrained by their

13 low charge/discharge stability and sloping voltage since the electron transfer is controlled by

14 the concentration of dopant (10~50%)[1]. Their π-conjugated backbone structures, arising from

15 alkene bonds or aromaticity, are more rigid than linear aliphatic polymers, thus restrict the

16 rotation and movement of the polymer chains and generally results in brittleness and poor

17 processibility of the polymers.

18 Polymer-based composites are highly desirable compared to bulk polymer materials as a

19 result of their synergistic combination of low temperature manufacturing processes, low

20 density and multiple functionalities. The addition of functional fillers, such as carbon-based

21 nanomaterials, ceramic fillers or metallic powders, can introduce charge- and heat-conduction

22 functionality to polymers. These have extended the application of polymer composites to a

23 broad range of uses, such as electrostatic dissipation (ESD) apparatus, electromagnetic

24 interference (EMI) shielding, electrostatic paint for panels, conducting adhesive, resistors,

25 piezo-resistive gauges[2, 3], supercapacitors[4, 5], lightning strike protection, electro-optical

1   devices, packaging for electronic devices[6] and bipolar plates for fuel cell applications[7].

2   However, the enhancement of the electrical- or thermal-conductivity of polymer composites

3   are limited by the dispersion, morphology and interfacial interaction between the filler and

4   polymer. The electrical conductivity normally reaches saturation above a certain filler loading

5   (percolation threshold), and the presence of electrically conducting fillers can also increase

6   the thermal conduction, which is undesirable in some applications, such as organic light-

7   emitting diodes. Developing approaches to maximize the electrical or thermal conductivity of

8   polymer composites without compromising processibility and mechanical properties

9   continues to be technical challenges.

10   To date, three approaches have been investigated to tackle the above challenges. This first

11   approach is to combine different types of particles, i.e., the 'hybrid-filler' approach, which

12   includes the combination of particles with different structures, dimensions, aspect ratios and

13   physical properties. A second approach involves the selective localisation of fillers in

14   different phases of polymer blends. In this case the electrical conductivity of polymers can be

15   enhanced through the formation of dual- or triple- percolated structures within the polymer

16   matrix. The selective localisation of the fillers at the interfaces of co-continuous polymer

17   structures can further reduce the amount of filler required to form a percolated network. A

18   third approach utilising a segregated structure and thermal annealing has proven to be

19   effective in producing highly electrical or thermal conducting polymer composites.

20   Polymer composites with high electrical conductivity at low filler loadings are desirable for

21   lightweight applications since they provide an opportunity to replace metal- or graphite-based

22   bipolar plates for fuel cell applications[8, 9], and allow for the manufacture of flexible and

23   stretchable electronics and sensors[10, 11, 12]. In this article, a critical review of the latest

24   development and a variety of the modification strategies for electrical or thermal conductive

1   polymer composites is presented, the relevant theoretical models for electrical and thermal

2   conduction of polymer composites with single and multiple filler systems are discussed.

3   **2. Electrical conductivity of polymer composites**

4   *2.1 Conductive filler dispersion and the percolation threshold*

5   The electrical resistivity (ρ) of a material is a measure of its resistance to an electrical current,

6   measured in Ohm·cm (Ω·cm). The inverse is electrical conductivity (σ), $\sigma = 1/\rho$, measured in

7   Siemens/cm (S/cm).

8   Most polymers are electrical insulators with σ of $10^{-14} \sim 10^{-18}$ S/cm. The addition of highly

9   electrically conductive fillers ($10 \sim 10^5$ S/cm) to polymers can facilitate charge transport

10   through electron hopping or tunnelling once a percolated conductive filler network is formed

11   throughout the polymer matrix. The critical filler concentration, at which an insulator-to-

12   conductor transition occurs, is termed as percolation threshold (φ_c), which is dependent on the

13   type, shape, dimensionality and orientation of the conductive filler(s), as well as their

14   thermodynamic and kinetic interactions with polymers[13]. A low φ_c is preferable

15   considering the processing, mechanical properties and cost of the polymer composites.

16   The materials that have been used to enhance the electrical properties of polymers include

17   carbon based materials such as 0-D carbon black (CB), 1-D carbon fibre (CF) and carbon

18   nanotubes (CNTs), 2-D graphite and graphene[14]; metal powders in the form of metal

19   oxides such as aluminium (Al), nickel (Ni), iron (Fe), copper (Cu) and silver (Ag)-based

20   fillers, as well as metal particle coated fillers such as Fe-doped CNTs or Ag-coated cellulose

21   whiskers.

22   To achieve a high electrical conductivity at low filler loadings, the dispersion and distribution

23   of fillers in the polymer matrix are critical. Dispersion refers to how the individual fillers

1   separate from each other. Due to the differences in surface energy and surface chemistry

2   between inorganic fillers and polymers, the inorganic fillers tend to agglomerate resulting in a

3   poor dispersion in polymer matrices. While the filler agglomerates may be well distributed

4   under the processing conditions, such as shearing, pressure or temperature[15, 16, 17].

5   Controlled and well dispersed fillers will increase the probability for filler-filler contacts[17,

6   18], however a good distribution of well-dispersed conductive particles will widen the gap

7   between the fillers, preventing conductive pathways from forming, thereby requiring a high

8   φ_c. As a result, constructing a three dimensional conductive network within an insulated

9   polymer matrix prefers a well-distribution of fillers, and not necessarily well-dispersed fillers.

10   Table 1 lists the electrical, thermal and physical properties of a range of typical fillers used in

11   polymers, including electrically conducting and dielectric fillers.

12   Table 1 Electrical conductivity (σ) and thermal conductivity (λ) values of commonly used

13   fillers[19, 20, 21, 22]

14

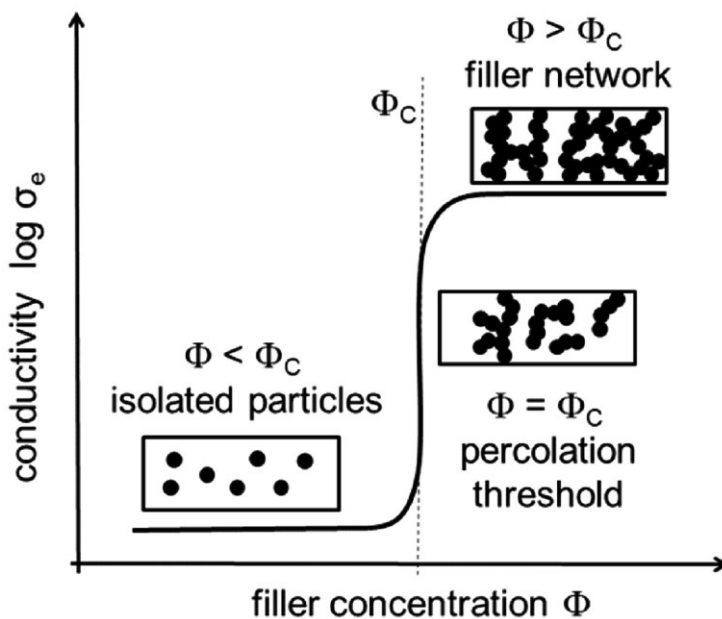| Filler type	Electrical conductivity (S/cm)	Thermal conductivity (W/mK)	Density (g/cm³)
Aluminium	3.54×10^5	234	2.7
Copper	5.98×10^5	386-400	8.9
Silver	6.31×10^5	417-427	10.53
Nickel	1.43×10^5	88.5	8.9
CNTs	3.8×10^5	2000-6000	2.1
CF	$10^2 \sim 10^5$	10-1000	1.5~2.0
Graphene	6000	4000-7000	1.06
Graphite	10^4	100-500	2.25
Expanded graphite	$<10^4$	1.17~45.33	0.002~0.005
Aluminium nitride	$<10^{-13}$	100-319	3.235
Beryllium oxide	-	230-330	3.025
Boron nitride	10^{-14}	185-400	2.27

15

16   When fillers are heterogeneously dispersed in a polymer, φ_c is typically reached within 10~30

17   vol% for dispersed metallic particles, 5~15 vol% for CB, and 0.1~3 vol% for CNTs or

18   graphene[23]. Conductive particles with a high aspect ratio and orientation tend to lead to a

19   low φ_c. For example, the φ_c of epoxy/multi-walled CNT (MWCNT) composites was

20   achieved at 0.02 wt% for long MWCNT of 350 μm, and 0.11 wt% for short MWCNT of 1.5

1   µm[24]. An extremely low φ_c of 0.0031 vol% was achieved when the CNTs were aligned

2   parallel in an epoxy, which is an order of magnitude lower than randomly orientated or

3   perpendicularly aligned CNTs[25].

4   At low filler concentrations, conduction is considered to occur via tunnelling between thin

5   polymer layers between the fillers [26]. As the filler loading increases, the filler particles

6   come into contact with each other to form a conductive network, which facilitates charge

7   transport within the composite, as shown in Figure 1. When $\varphi > \varphi_c$, the conductivity

8   increases sharply as a function of filler concentration, which can be modelled by a power-law

9   expression[27]:

10    $$\sigma = \sigma_f (\varphi - \varphi_c)^t \qquad (1)$$

11   where φ is the filler volume fraction, σ_f the filler conductivity, σ_c the composite conductivity,

12   t is a scaling exponent. The scaling exponent, t, is approximately 1.1~ 1.3 for two-

13   dimensional systems and between 1.6 ~ 2 for three-dimensional systems[28, 29]. More

14   scattered values of the exponent between 4 ~5 have also been reported[28, 29, 30, 31], which

15   are related to the microstructural properties of the composites.

16

1   Figure 1 Schematic percolation curve for the electrical conductivity of conducting fillers in

2   an insulating matrix and particle morphologies in the different distinguished regions.

3   Reprinted with permission [32]. Copyright 2016 Elsevier.

4   The difference of surface energies and surface chemistries between nanoparticles and

5   polymer matrices can often hinder the dispersion and distribution of the particles in polymers,

6   and the lack of interactions leads to the interfacial defects. Surface modification of the fillers

7   is generally employed to improve their dispersion in polymers. However, from a tunnelling

8   and conduction point of view, a relatively low interfacial interaction between CNTs and

9   polymers, coupled with partial agglomeration of CNTs was found to be beneficial for

10   improving the electrical properties of composites. In Figure 2 the higher affinity between

11   polyamide 6 (PA6) and CNTs attracts a thin insulting layer of PA6 to the CNTs surface,

12   which retards the formation of a conductive network of CNTs within PA6. In comparison, a

13   relatively poor interaction between polystyrene (PS) and CNTs leads to improved dispersion

14   and enhanced electrical conduction through the tunnelling mechanism[33].

15
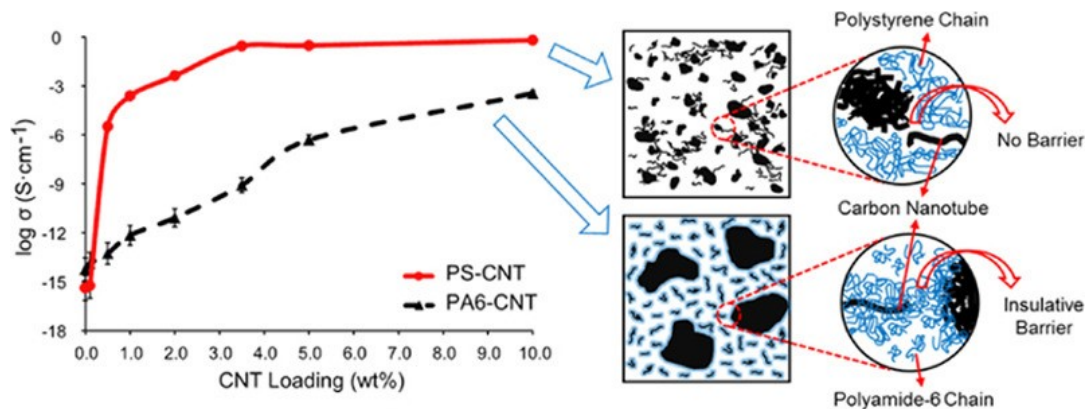
16

17   Figure 2 Effect of surface wetting of polymers to CNTs on the electrical conductivity of the

18   nanocomposites. Reprinted with permission [33]. Copyright 2017 Elsevier.

19   The maximum electrical conductivity of CNTs or graphene filled polymer composites is

20   generally lower than expected, despite the intrinsically high electrical conductivity of the

21   carbon nanoparticles, which is typically in the range of $10 \sim 10^5$ S/cm. The potential for a

1   tunnelling effect must be considered when an insulating polymer layer exists between

2   particles that leads to electrons hopping from one conductive cluster to another[30].

3   Tunnelling between CNTs in composites was estimated by the relationship between DC

4   conductivity and filler concentration, $log\sigma_{DC} \propto -\varphi^{-1/3}$[34]. The average tunnel distance d

5   among conducting particles in the composites depends on the filler loading, $d \propto \varphi^{-1/3}$[35],

6   and the distance is generally less than 5 nm[36].

7   *2.2 Hybrid filler system*

8   Conventional micro-scale fillers such as metallic particles, graphite, carbon black (CB) or

9   carbon fibres (CFs) generally improve the electrical conductivity of polymers at

10   concentrations up to 65~80 vol%[37], with maximum conductivities in the range of 0.1~20

11   S/m. However, the high concentrations of fillers inevitably deteriorate the mechanical and

12   processing properties of the polymers.

13   The addition of a second filler can potentially balance processing properties and generate

14   synergistic effects [38, 39, 40]. The second filler can be either conducting or insulating, such

15   as nano-clay, cellulose nanocrystals or silica particles. The presence of insulating nanosized

16   fillers may assist the dispersion and bridge the conducting fillers and helps reduce the

17   electrical percolation threshold. These combinations of fillers will now be discussed.

18   *2.2.1 Combination of electrically conductive fillers*

19   In order to couple the effects of nano- and micro-scale fillers, composites of epoxy containing

20   micro-scale short carbon fibers (SCFs) and CNTs were prepared via a two-step procedure,

21   using an epoxy/CNTs composite as the matrix, and incorporating SCFs as the second

22   filler[41]. As shown in Figure 3, the effective electrical conductivity (σ_{eff}) of the SCF-CNT-

23   epoxy composites increased with an increase of SCF concentration. By using a high aspect

1 ratio SCF ($\xi_{SCF} \geq 50$), an electrical conductive network was formed at low volume fractions,

2 and σ_{eff} was approximately two orders of magnitude higher than composites containing SCF

3 with a low aspect ratio ($\xi_{SCF} \leq 10$). Therefore, increasing the aspect ratio of the SCF is more

4 effective in increasing σ_{eff} than increasing the volume fraction.
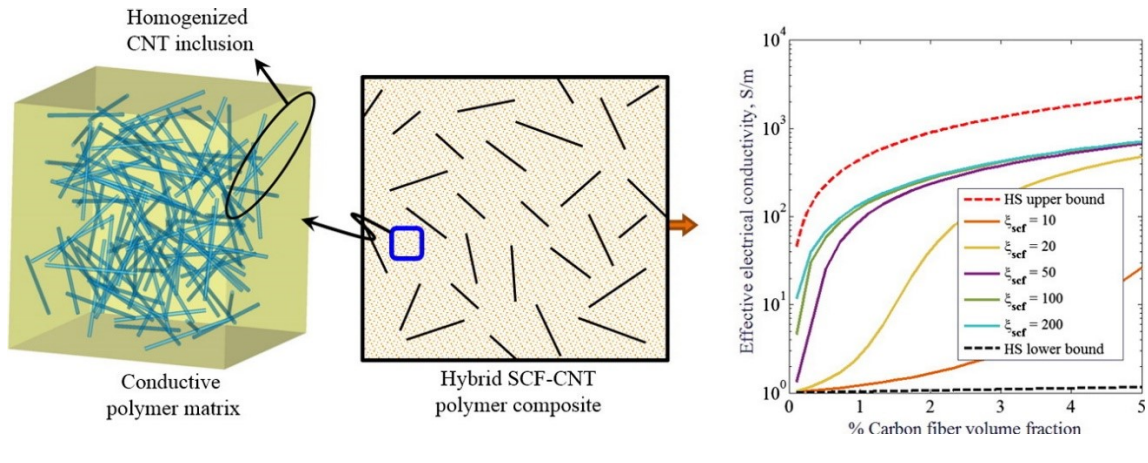
5
6

7 Figure 3 Schematic of composites of polymers and both SCFs and CNTs and, the effect of

8 SFC aspect ratio on electrical conductivity. Reprinted with permission from Pal et al[41].

9 Copyright 2016 Elsevier.

10

11 On comparing the in-plane and through-plane electrical conductivity, the highest conductivity

12 for a single filler composite system epoxy (bisphenol-A type)/synthetic graphite (80 wt%)

13 was 53 S/cm for the in-plane conductivity while the through-plane conductivity was 40 S/cm.

14 The addition of 2 wt% milled CFs increased the in-plane conductivity to 69.8 S/cm, and the

15 through-plane conductivity to 50.3 S/cm[42]. For the epoxy (bisphenol-F type)-based

16 composites containing three different combinations of reinforcements, i.e., graphite-CB,

17 graphite-MWCNT and graphite-CF[39], a maximum conductivity of 255 S/cm was obtained

18 for the composite containing 73 vol% graphite, 2 vol% CNT with 25 vol% epoxy matrix. The

19 incorporation of CNT in the epoxy(bisphenol-A type)-graphite composites substantially

20 improved the electrical conductivity by 105%, and the flexural strength of the composites

21 were also improved by 173%. When using milled CFs as the primary conductive filler[43],

1   the addition of CNTs provided higher through-plane conductivity of 40.3 S/cm than that with

2   CB at 19.9 S/cm. This indicates that the combination of CNTs with higher aspect ratio CF

3   provides higher conductivity. Moreover, this study revealed that the combination of

4   graphite/CNT provides higher electrical conductivity than that of CF/CNT.

5   Hybrid filler systems also facilitate the dispersion of the fillers and form an interconnected

6   conductive network in thermoplastic polymers. For composites of polypropylene (PP)/CB,

7   the addition of 8 wt% CF into CB/PP, higher conductivities were obtained for the CF/CB/PP

8   beyond the percolation region, compared with the CB/PP or CF/PP composites. This suggests

9   that a conductive network was formed where the CF forms a long conductive pathway, and

10   CB particles bridges the CFs[44], the resultant composites demonstrated superior liquid

11   sensing properties [45]. For hybrid CNT-CB fillers modified polyamide 12 (PA 12)

12   composites, the $\varphi_c = 0.9$ wt % was obtained which was similar to the single filler modified

13   PA12 composites. While the additional CB particles improved the dispersion of CNTs, and

14   resulted higher electrical conductivity[46].

15   The dispersion and electrical conductivity of polymer composites are also effected by the

16   processing methods, some examples are shown in Table 2.

17   PP/nickel-coated CF (Ni-CF) (70/30, wt%) composites prepared by injection moulding

18   demonstrated the highest electrical conductivity of 17.5 S/cm and EMI shielding

19   effectiveness (SE) of 48.4 dB at a frequency of 10 GHz, respectively. The EMI SE shows the

20   capacity of the materials to dissipate electromagnetic energy, and is generally expressed in

21   decibels (dB)[47]. The enhancement in real and imaginary dielectric constants (ε' and ε'')

22   were related to the percolation at a lower Ni-CF concentration, which was affected by the

23   increased CF length (orientation) in the composite prepared by the injection moulding

24   process[48] .

1   In comparison to traditional melt-mixing, a more homogeneous dispersion of nanofillers at

2   high concentrations can be achieved by *in situ* polymerisation. For example, chemically

3   expanded graphite (CEG) with a large specific surface area (>840 m^2/g) was exfoliated into

4   single- and few-layer graphene in the poly(methyl methacrylate) (PMMA) matrix when the

5   polymerisation occurred in between the graphite layers[49]. When the graphene

6   concentration was 10 wt%, the electrical conductivity of the composites was significantly

7   enhanced to 1719 S/m, due to the dense graphene network with thinner PMMA insulating

8   layers. In addition, the elastic modulus exhibited a three-fold increase compared to pure

9   PMMA. Therefore, with th surface-modified nanofillers, *in situ* polymerisation makes it

10   possible to achieve a good dispersion and high electrical conductivity at relatively high

11   graphene concentrations.

12   Composites of PS/MWCNTs/graphite nanoplatelet (GNP) were prepared by *in situ*

13   polymerization of styrene/CNTs in the presence of PS/GNP microbeads. An electrical

14   conductivity of 9×10^{-3} S/cm was achieved for GNP and MWCNT loadings of 0.29 and 0.3

15   wt%, respectively. A high EMI shielding value (~20.2 dB) was achieved at low MWCNTs

16   (~2 wt%) and GNP (~1.5 wt%) concentrations. The high electrical conductivity and high

17   EMI shielding were associated with the continuous conductive network structure of CNT-

18   GNP-CNT and the strong π-π interactions (i.e., the interactions between aromatic groups

19   caused by the sharing of delocalised electrons into empty p-orbitals) among the phenyl rings

20   of PS with GNP and CNTs[35].

21   For composites of PS/reduced graphene oxide (rGO)/CNTs prepared by a vacuum

22   impregnation polymerisation[50], when the initial GO mass was increased to 30 mg

23   (GO:CNTs=2:1), the electrical conductivity of rGO/CNTs/PS composites was enhanced by

24   11 orders of magnitude relative to pure PS. This was associated with the hierarchical

25   rGO/CNTs structure that formed a continuous conductive pathway in the polymer matrix.

1   For composites of poly(vinylidene fluoride) (PVDF)/MWCNT/GNP prepared by a solution

2   mixing method, the electrical conductivity and the EMI shielding properties of the

3   composites increased with increasing filler loading. Moreover, the EMI shielding properties

4   of the PVDF/MWCNT/GNP composites were greater than composites of either PVDF/CNT

5   or PVDF/GNP. The total shielding of PVDF/CNT/GNP films increased from 21.90 to 36.46

6   dB as the film thickness increased from 0.06 to 0.25 mm. The PVDF/carbon composite films,

7   with a thickness of 0.1 mm, achieved the highest specific shielding values of 1310 dB cm^2/g

8   for a PVDF/5 wt %-CNT composite and 1557 dB cm^2/g for the PVDF/CNT/GNP composite.

9   The specific SE (dB cm^2/g) is defined as SE divided by the mass density and thickness[51],

10   and is a crucial criterion for high-efficiency shielding materials. This indicates that the hybrid

11   filler approach is promising for generating flexible and ultra-thin conductive polymer

12   composite films[52], where EMI shielding properties could be tuned by controlling the film

13   thickness.

14   Graphene and MWCNTs were incorporated into poly(*p*-phenylenebenzobisoxazole) (PBO)

15   via *in situ* polymerization of functionalized PBO precursor with GO/MWCNTs, followed by

16   high-temperature carbonization [53]. The reflection loss of PBO composites containing 7.5

17   wt% of reduced GO/MWCNTs was -50.17 dB at 12.58 GHz, over 20 times higher than that

18   of pure PBO (-2.33 dB at 12.58 GHz) with a sample thickness of 2.6 mm. These composites

19   also exhibited highly improved microwave absorption properties and good thermal stability

20   compared to the unfilled PBO.

21   The combination of GO with CNTs helps isolate CNTs bundles and stabilise CNTs in

22   aqueous PS latex by forming a GO-CNTs shell on PS sphere surfaces. The GO-CNTs layers

23   were thermally reduced to rGO-CNTs during compression moulding of the PS latex spheres

24   and formed a 3D foam-like conducting network structure, as shown in Figure 4. This

1   composite exhibited an ultra-low φ_c of 0.03 vol% rGO-CNTs and a high electrical

2   conductivity of 1.53 S/cm at 4 vol% rGO-CNTs[54].
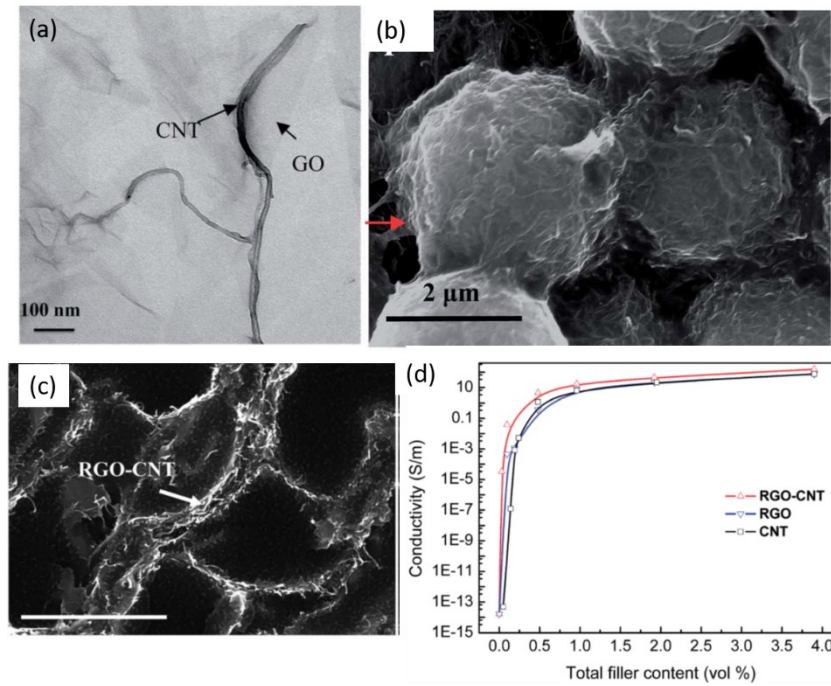
3

4   Figure 4 (a) TEM image of GO-CNT dispersion after drying; (b) SEM image of rGO-

5   CNT/PS microspheres; (c) cross-sections of PS composites containing 2 vol% rGO-CNTs;

6   and (d) electrical conductivity of PS composites as a function of filler content. Reprinted with

7   permission from Tang et al[54]. Copyright 2014 Royal Society of Chemistry.

8   *2.2.2 The addition of a second insulating filler*

9   The addition of 30 wt% electrically insulating $CaCO_3$ to PP/CNT composites reduced φ_c from

10   6.2 to 3.6 wt%, increased electrical conductivity from 10^{-7} to 10^{-2} S/m at 9 wt% CNT, as well

11   as increased the notched impact strength of PP from 16 to 33.1 kJ/m^2, as shown in Figure 5.

12   The $CaCO_3$ provides a volume-exclusion effect to the composite, and leads to a denser

13   interconnecting CNT network and higher electrical conductivity[55].
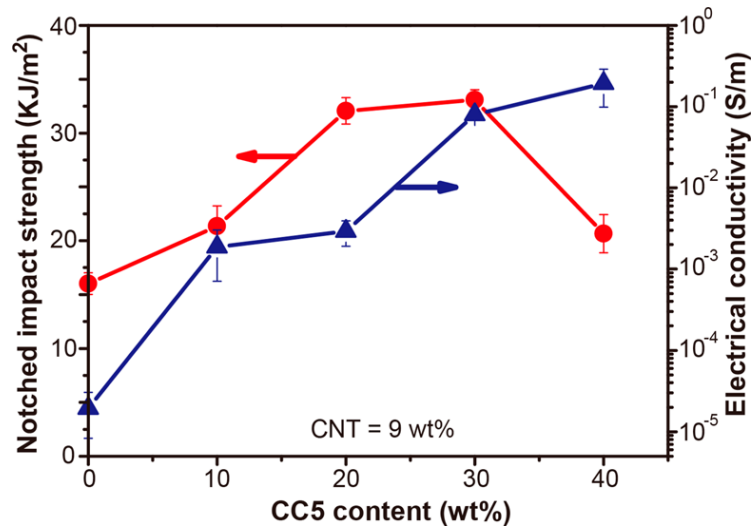
1

2 Figure 5 Notched impact strength and electrical conductivity versus $CaCO_3$ content for

3 composites. Reprinted with permission from Li et al[55]. Copyright 2017 American

4 Chemical Society.

5

6 When mixing of cellulose nano-whiskers (CNs) and CB particles in composites, the CB can

7 arrange along the long-axis surface of CNs, yielding a conductive structure with a high aspect

8 ratio. As shown in Figure 6, natural rubber (NR) composites containing a hierarchical

9 conductive CB-CN network showed $\varphi_c = 2.9$ vol%, much lower than the CB/NR composites

10 (7.3 vol%). The electrical conductivity was enhanced by 12 orders of magnitude at 5 vol%

11 CB, compared to the rubber matrix, and the tensile strength was increased by 760% for the

12 CB-CN filled rubber composites (CB@CNs/NR)[56].
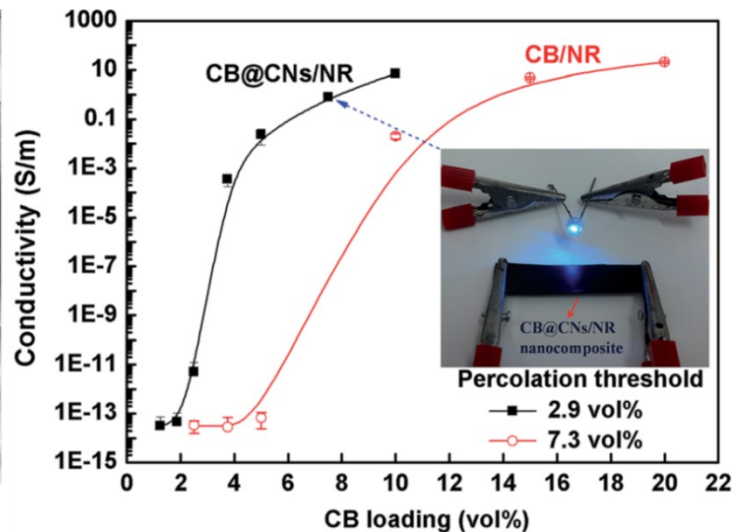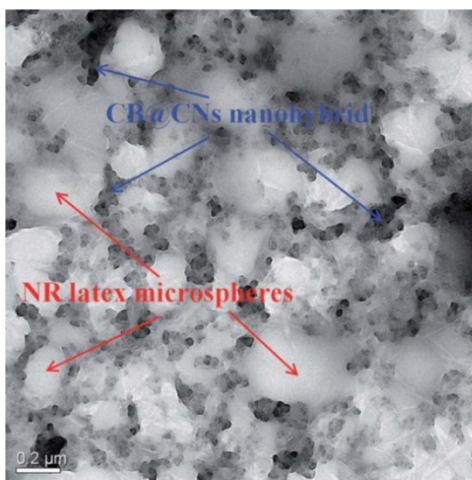
13

1 Figure 6 TEM image of the CB-CNs/NR composite prepared by self-assembly of CB@CNs

2 and NR latex and electrical conductivity as a function of CB content. The inset shows a CB-

3 CNs/NR composite (7.5 vol% filler loading) lighting an LED device. Reprinted with

4 permission from Wu et al[56]. Copyright 2015 Royal Society of Chemistry.

5

6 A combination of two types of fillers with large aspect ratios, such as CNTs with nano-

7 fibrillated cellulose (NFC, approximate diameters of 2-5 nm and lengths of 3-5 μm)

8 significantly enhanced the electrical conductivity and mechanical properties of a

9 thermoplastic polyurethane (TPU) as compared to the single filler system[57]. The addition

10 of NFCs assisted the dispersion of the CNTs in the TPU, and reinforced the TPU due to

11 strong interfacial interactions between the amphiphilic NFC and TPU. The electrical

12 conductivity of TPU/NFC@CNTs composites increased with the NFC concentrations and

13 reached 0.28 S/m with 3 wt% NFC and 1 wt% of CNTs, compared with 0.0012 S/m for

14 TPU/CNT composites. A high stretching sensitivity with a gauge factor of 50 was achieved

15 which was ascribed to the extended length (overall aspect ratio) of the CNTs in combination

16 with the longer NFC, as shown in Figure 7.
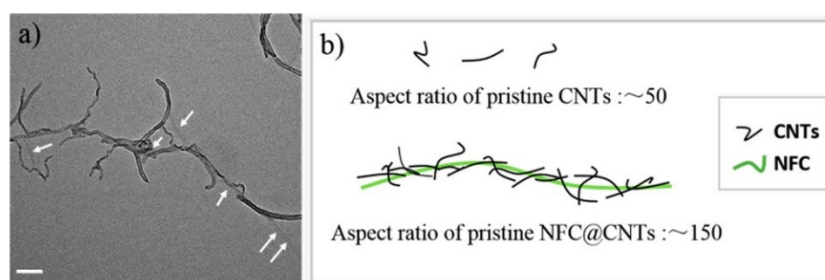
17
18

19 Figure 7 (a) TEM image and (b) Schematic of nano-hybrid fillers of CNTs and nano-

20 fibrillated cellulose (NFC). Reprinted with permission from Xu et al[57]. Copyright 2017

21 American Chemical Society.

22

Table 2 Electrical properties of polymer composites, hybrid filler versus single filler

Matrix	Single filler	Secondary filler	Filler ratio	Dispersion technique	Percentage filler to reach percolation threshold		Max. conductivity S/cm @ filler concentration		Reference
					Single	Hybrid	Single	Hybrid	
Epoxy (bisphenol-F type)/	Graphite	CB	70:5 vol%	High speed mixer			124 @75 vol% graphite	153 @ 70 vol% graphite+5 vol%CB	[39]
	Graphite	MWCNT	73:2 vol%	High speed mixer			124 @75 vol% graphite	254@73 vol% graphite+2 vol%MWCNT	
	Graphite	CF	68:7 vol%	High speed mixer			124 @75 vol% graphite	235@68 vol% graphite+7 vol%CF	
PEBA	Graphite(GNP)	HS-CB	2.45: 1.05 wt%	Melt mix	6.7 vol%	3.5 vol%			[58]
PEBA	LS-CB	GNP	1.18:4.72 vol.%	Melt mix	11.7 vol%	5.9 vol%			
PPS	Graphite	CB	70 : 9 wt%	Melt mix			73@ 80 wt% graphite	140 @ 70 wt% graphite+9 wt%CB	[37]
PPS	Graphite	CNTs	80: 3 wt%	Melt mix			73@ 80 wt% graphite	75@ 80 wt% graphite+3wt%CB	
PA12	CB	CNTs	0.9: 0.9 wt%	Melt twin screw	4.3 wt%	1.2 wt%			[46]
PS	CF	CB	1.18:0.71 vol%	Melt twin screw	8 vol%	1.9 vol%			[44]
Epoxy (bisphenol-A type)/	Graphite	MCF	78:2 wt%	Melt mix			53@ 80 wt% graphite	69.79@ 78 wt% graphite+2wt%MCF	[42]
PP	CB	CF	14.1:8 wt%	Melt mix	14.1 wt%	12.5 wt%			[45]
COC	CF	EG	14.2:8.3 vol%	Melt mix twin screw			1.2×10^{-2} @60 phr CF	6.3×10^{-2} @40 phr CF +20 phr EG	[59]
PS	rGO	CNTs	2:1 wt%	Vacuum impregnation				1.21×10^{-5}@ 0.6wt% rGO + 0.6wt% of CNT	[50]
Epoxy	CF	CNTs	72:6 wt%	Melt compounding			6.34 @80wt% CF	40.3 @ 6wt% CNT + 72wt% CF	[43]

(bisphenol-A type)/	CF	CB	78:2 wt%	Melt compounding			6.34 @80wt% CF	19.9 @ 2wt% CB + 78wt% CF	
Resole phenol formaldehyde	NG	CB	70:5 vol%	Compression molding				115.71@70 vol% NG+ 5 vol% CB	[60]
epoxy resin	CF	SWNT		Chemical vapor deposition			0.022	0.049 @0.25wt% SWNT	[61]
(EPON 862)	CF	MWNT		Chemical vapor deposition			0.068	0.089@0.25wt% MWNT	

2.3 Selective location of fillers in polymer blends

Most polymers are thermodynamically incompatible with each other due to the difference in chain structures and configurations, which is related to the unfavourable enthalpy of mixing and non-negligible entropy [62]. Consequently, polymer blending normally leads to heterogeneous systems with a range of multi-phase morphologies. In a two-phase immiscible polymer blend, one polymer phase at lower concentration or higher viscosity tends to be dispersed as droplets in the major phase, leading to a 'sea-island' morphology. The increase of polymer phase ratios or selective dispersion of fillers in one phase, can induce a transition from 'sea-island' morphology to co-continuous morphology, and even phase reversion [63, 64]. At the phase reversion point, the two immiscible phases remain continuously connected throughout the bulk of the blend[65].

The localisation of fillers in polymer blends depends on the viscosity of the polymers and interfacial energies between blend components. Theoretically, once thermodynamic equilibrium is achieved, the localisation of fillers in polymer blends can be determined by minimizing the interfacial energy[66, 67]. According to Young's equation[68, 69], the thermodynamic equilibrium for the localisation of fillers in polymer blends can be estimated from wetting coefficient (w_a), $\omega_a = \frac{\gamma_{f-A} - \gamma_{f-B}}{\gamma_{A-B}}$, where γ is the interfacial energy between different components, i.e., fillers (f), polymers A and B. When $\omega_a < -1$, the filler is located preferentially in phase A; $-1 < \omega_a < 1$, the filler is located at the interface between phase A and B, while when $\omega_a > 1$, the filler is located preferentially in B phase.

Two different approaches are used to calculate the interfacial energy, γ_{ij}. For a high surface energy material the mean harmonic approximation is used[68, 70],

$$\gamma_{ij} = \gamma_i + \gamma_j - 4\left(\frac{\gamma_i^d \gamma_j^d}{\gamma_i^d + \gamma_j^d} + \frac{\gamma_i^p \gamma_j^p}{\gamma_i^p + \gamma_j^p}\right) \qquad (2)$$

while for low surface energy materials the geometric mean approximation is applied,

$$\gamma_{ij} = \gamma_i + \gamma_j - 2\left(\sqrt{\gamma_i^d \gamma_j^d} + \sqrt{\gamma_i^p \gamma_j^p}\right) \qquad (3)$$

In both equations, γ^d and γ^p are the dispersive and polar components of the surface energy of the component, respectively.

The electrical conductivity of polymer composites can therefore be tailored by varying either the conductive filler loading or the phase morphology. The selective localization of the filler in one phase of immiscible polymer blends, or at the interfaces of sea-island or co-continuous phases provides a composite with the lowest φ_c, if the interfacial region is continuous. Further examples are listed in Table 3. The double percolation phenomenon was firstly proposed by Sumita et al[69], where the percolation of conductive particles in one phase, enables percolation of the immiscible phases throughout the whole composite.

2.3.1 Selective localisation of fillers in sea-island structured polymer blends

For PLA/PU (85/15 wt%) blend, the minor PU phase is dispersed in the continuous PLA phase and forms a sea-island phase morphology, as seen in Figure 8a [63]. The addition of CB particles with concentrations from 1 to 3 phr (i.e. parts per hundred rubber) induced a gradual expansion of the PU droplets which eventually connected to form a continuous-like morphology, where the CB was only located in the PU phase, see Figure 8b. The self-networking ability of the CB particles and the co-continuity of the polymer phases contributed to enhancements of impact strength by 291% and electrical conductivity up to 5.78×10^{-3} S/m, see Figure 8c,d. Similar phenomena were observed in MWCNTs filled

PP/PS (90/10 vol%) blends[67]. The localisation of MWCNT in both the PS minor phase and at the interface induced a phase transition from a dispersed to co-continuous morphology. This was due to slowing down of the relaxation dynamics of PS/MWCNT; and the MWCNT located at the interface acted as a bridge favouring coarsening of the PS/MWCNT. The percolation of the composites of PP/PS (50/50) and PP/PS (90/10) occurred at MWCNT concentrations of 0.5 and 1.0 vol%, respectively. Therefore, the selective localisation of fillers in the minor phase of a polymer blend can induce a double-percolated structure and lead to enhanced electrical conductivity.
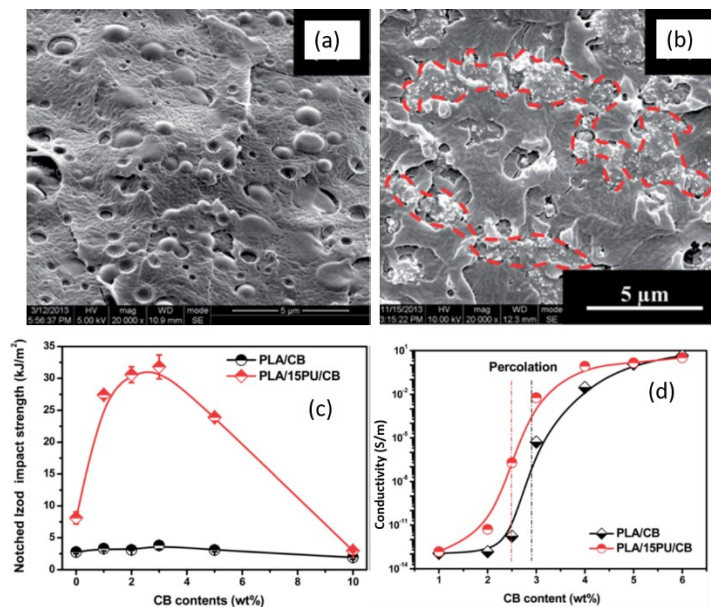

Figure 8 SEM images of (a) PLA/PU (85/15) and (b) PLA/PU/CB (85/15)/3phr, (c) Notched Izod impact strength and (d) electrical conductivity of neat PLA and PLA/15PU blend with various CB content. Reprinted with permission from Xiu et al [63]. Copyright 2017 Royal Society of Chemistry.

In the case of 'sea-island' structured polyurethane (TPU)/polyamide copolymer (COPA) blend (80/20 wt%), CB particles were found to be preferentially located at the interface of the blend irrespective of the compounding sequences employed, as shown in Figure 9. The CB particles interact with both phases through hydrogen bonding and act as Janus particle-type compatibilizers. The φ_c of TPU/CB was reduced from 6.9 vol% to 3.7 vol% after addition of

COPA, suggesting the COPA assisted the formation of a conductive pathway, and provided a narrower tunnelling distance for electrons[71].
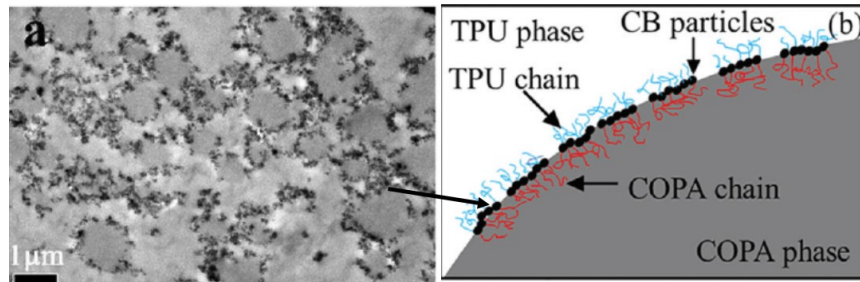

Figure 9 (a) The formation of a conductive CB network in TPU as a result of COPA addition, and (b) illustration for interfacial localization of Janus-like CB particles in the TPU/COPA blend. Reproduced with permission from Zhang et al[71]. Copyright 2017 Royal Society of Chemistry.

2.3.2 Selective localisation of fillers in co-continuous structured polymer blends

To selectively localise conductive fillers at the interfaces of co-continuous structures, the fillers can be surface-treated to exhibit affinity to both phases thermodynamically, or by tailoring the processing sequences [71, 72, 73, 74].

A typical co-continuous phase morphology was observed in a PS/PMMA (50/50 wt%) blend. The surfaced treated MWCNTs containing carboxylic groups were observed to selectively disperse at the interface of PS/PMMA (50/50 wt%) blends. The dispersion of MWCNTs were affected by balancing the dipole-dipole interactions of –COOH with the PMMA phase and the π-π interaction between the MWCNTs and PS. An optimised carboxyl content on the MWCNT surfaces was 0.73 wt%, which can precisely place the MWCNTs at the co-continuous PS/PMMA interface to form a percolated conductive pathway. A low φ_c was obtained at 0.017 wt%, while it was 1.81 wt% for a PS/MWCNTs composite and 1.46 wt% for the PMMA/MWCNT composites, see Figure 10a[75].

GO nanosheets bearing surface-grafted random P(S-co-MMA) copolymer selectively dispersed at the interface of immiscible PS/PMMA (50/50 vol%) blends, and resulted an ultra-low φ_c of 0.02 vol%. The covalently grafted copolymer on the GO surface enhanced the interfacial compatibility among the graphene sheets and the polymer blends, see Figure 10b[76].

In another system, octadecylamine-functionalized graphene (GE-ODA) was exclusively located in the PS phase in PS/PMMA blends, independent of the component ratio and processing conditions. For the PS/PMMA blend (50/50 wt%), a φ_c of 0.5 wt% was achieved and the electrical conductivity was enhanced by six orders of magnitude compared to the PS/GE-ODA composite due to the formation of a percolated network of graphene sheets in the continuous PS phase, see Figure 10c[77].
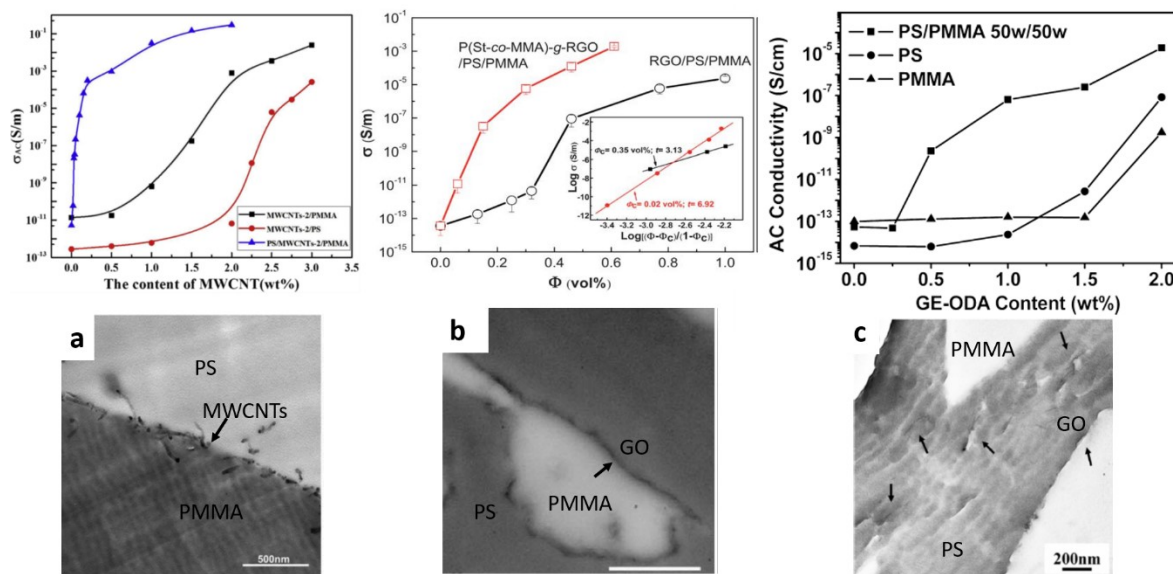

Figure 10 (a) AC conductivity (at 1 Hz) of MWCNT/PMMA, MWCNT/PS and PS/MWCNT/PMMA (40/60 wt%) composites as a function of MWCNT content and a TEM image of the 0.5 wt% MWCNT filled PS/PMMA blends. Reprinted with permission from Chen et al[75]. Copyright 2017 Elsevier; (b) DC conductivity as a function of filler content for rGO and P(S-co-MMA)-g-rGO filled PS/PMMA (50/50 vol%) blends and a TEM showing dispersion of 0.46 vol% rGO in the PS/PMMA blend. Reprinted with permission from Tan et al[76]. Copyright 2013 Royal Society of Chemistry; (c) AC conductivity (1 Hz)

vs GE-ODA loading in PS/PMMA (50/50 wt%) blend, PS and PMMA and a TEM image of PS/PMMA (50/50 wt%) blends filled with 1.0 wt% GE-ODA. Reprinted with permission from Mao et al[77]. Copyright 2012 American Chemical Society.

Instead of covalently modification of CNTs, a poly(styrene-ethylene-methyl methacrylate) triblock terpolymer (PS-b-PE-b-PMMA) was applied to physically modify CNTs. The ethylene middle block was selectively adsorbed onto the CNT surface, and the immiscible PS and PMMA end blocks were phase-separated into a patchy PS/PMMA blend, as shown in Figure 11. Such modified CNTs were dispersed homogeneously in both phases and at the interfaces as a result of the adaptable morphology of the patchy corona blocks. This provides a novel route for highly selective localisation of CNTs in multiphase polymer blends, although no electrical properties were reported in this work[78]
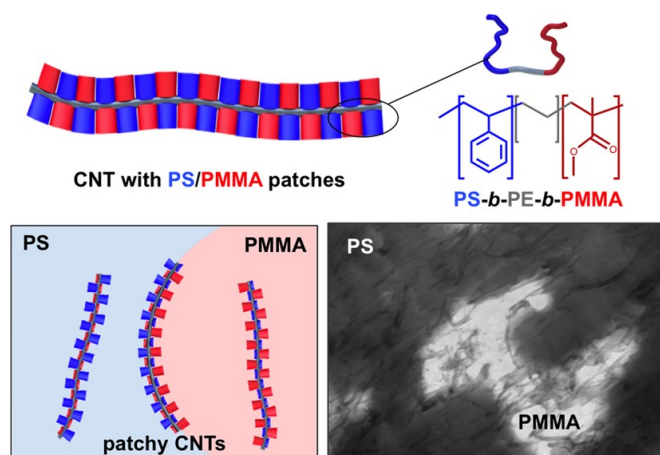

Figure 11 Patchy CNTs and the distribution in PS/PMMA blends. Reprinted with permission from Gegenhuber et al[78]. Copyright 2016 American Chemical Society.

In poly(ethylene vinyl acetate)/thermoplastic polyurethane (EVA/TPU) blend, MWCNTs were only located in the TPU phase, independent of the phase ratios. A dielectric percolation threshold was observed for EVA/TPU (80/20) containing between 3 and 5 wt% MWCNTs leading to a sharp increase in the dielectric constant from 85 to 100 at 1200 Hz, see Figure 12. This was because the MWCNTs filled TPU droplets were isolated by thin EVA layers,

forming a network of micro-capacitors, which induced greater charge accumulation on the interfaces of the TPU and EVA phases due to the increased interfacial polarization, resulting in an increase in AC conductivity. A 3D double percolated structure was formed for co-continuous EVA/TPU (50/50) blends. Compared to the sea-island morphology, the dispersion of MWCNTs at the interface diluted its concentration in the TPU phase, and thus reduced the number of micro-capacitors generated by neighbouring MWCNTs. In this case, the blend with sea–island morphology is beneficial for high dielectric constant and low dielectric loss[79].
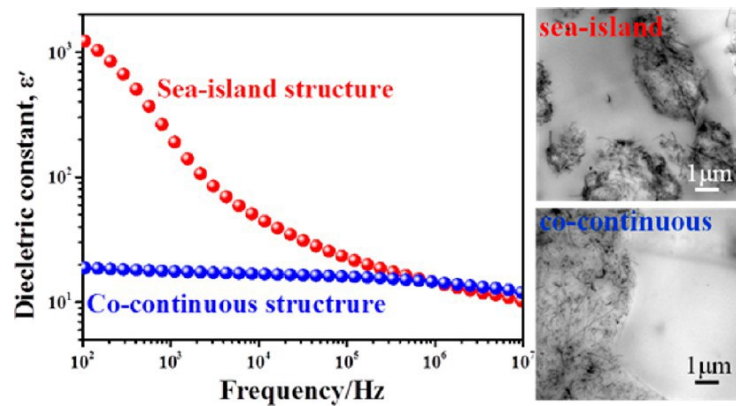

Figure 12 Dielectric constant of composites with different morphologies as a function of frequency, and the associated TEM images. Reprinted with permission from Zhang et al[79]. Copyright 2017 American Chemical Society.

The selective localisation of particles also depends on their aspect ratio. A high aspect ratio facilitates dynamic transfer of the fillers across the interface and lowers the stability of the filler in the interface region. Therefore, the selective localisation of low aspect ratio CB particles at the interface is often reported[80]. For example, in co-continuous PS/PMMA (50/50 vol%) blends, CB was preferentially localised in the continuous PS phase, which suppressed phase coarsening during quiescent annealing, and also resulted in a double percolation threshold at half of the value attained for a single-phase composite[80].

The nanofillers can be brought to the interfaces of polymer blends by addition of a third

polymer as a compatibiliser. In CB filled PP/PS (70/30 vol%) blends[71, 74], the presence of 5 vol% of a styrene–butadiene–styrene (SBS) copolymer attracted the CB particles to migrate from the PS phase to the interface with the PP matrix due to its higher affinity to CB fillers. This reduced the φ_c of the composites from 1.55 to 0.95 vol%.

When MWCNTs were initially melt-mixed with a PS-r-PMMA random copolymer, then melt-mixed with a partially miscible blend of poly-a-methylstyrene-coacrylonitrile (PaMSAN) and PMMA (85/15 wt%), it was found that the MWCNTs were mainly dispersed at the interface and bridged the PMMA droplets (Figure 13a). It was proposed that upon phase separation, the MWCNTs migrate to the interface mediated by PS-r-PMMA. The MWCNTs bridged the PMMA droplets and resulted in an interconnected network-like structure. The PaMSAN/PMMA (85/15) containing PS-r-PMMA modified MWCNTs exhibited a moderate electrical conductivity of 10^{-7} S/cm, and a low electrical φ_c of 0.25 wt% [81]. The conductivity was further increased by approximately two orders of magnitude upon annealing, see Figure 13b.
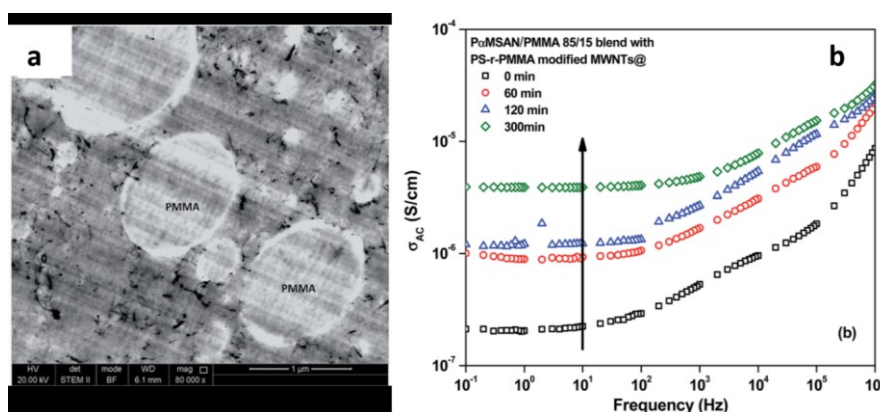

Figure 13 (a) PaMSAN/PMMA (85/15 wt%) blends with PS-r-PMMA modified MWNTs; (b) PS-r-PMMA modified MWCNTs. The effective concentration of MWCNTs is 0.25 wt%. Reprinted with permission from Bose et al[81]. Copyright 2016 Royal Society of Chemistry.

A different strategy can be demonstrated by examining MWCNTs filled poly(lactic acid) (PLA)/poly(ε-caprolactone) (PCL) blends. The MWCNTs were firstly mixed with

thermodynamically unfavourable PLA, then added to PCL. The immiscible PLA/PCL blend

formed a co-continuous phase morphology at 50/50 wt% and the MWCNTs migrated from

the PLA phase towards the more favourable PCL phase during the melt-mixing process[73].

The second melt process was restricted to 4 min in order to trap the MWCNTs at the interface

before they entered into the PCL phase. A low φ_c of 0.025 wt% was achieved for the

PLA/PCL/MWCNT composites, see Figure 14. In comparison, PLA/PCL/MWCNTs

composites prepared by simultaneous mixing of the components had a higher φ_c of 0.97 wt%.

Therefore, the φ_c can be significantly reduced if the conductive fillers are selectively

distributed at the continuous interface of the co-continuous polymer blend, since only a very

small amount of fillers are required to form a conductive percolated network.
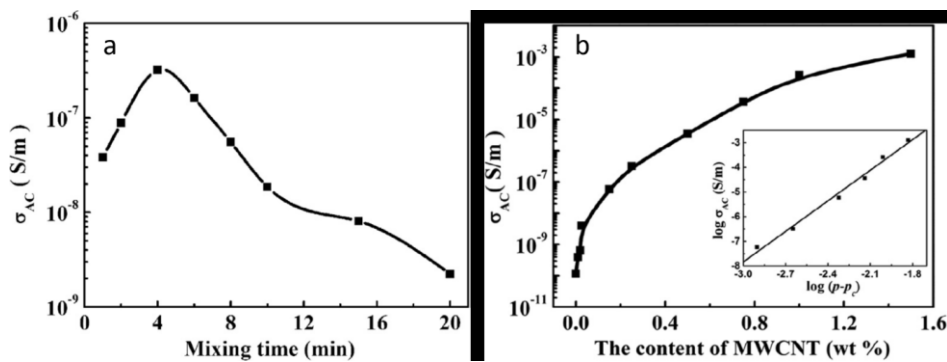

Figure 14 AC conductivity (at 0.1 Hz) of (a) PLA/0.25 wt% MWCNTs/PCL composites as a
function of mixing time, and (b) PLA/MWCNTs/PCL composites as a function of MWCNT
content. The mixing time was fixed at 4 min for all samples. Reprinted with permission from
Huang et al[73]. Copyright 2014 Elsevier.

Interfacial localisation of graphene in co-continuous polymer blends has been shown to be

effective in stabilizing the co-continuous morphology and increasing electrical conductivity

with a low electrical percolation threshold. By selectively locating thermally

reduced graphene oxide (rGO) at the interface of co-continuous PLA and PS blends, an

ultralow φ_c of 0.028 vol % was observed. It is believed that the rGO transfers from the PLA

phase to the interface during melt compounding and annealing, which forms a 3D network

that effectively suppresses the coarsening of the co-continuous structure[82].
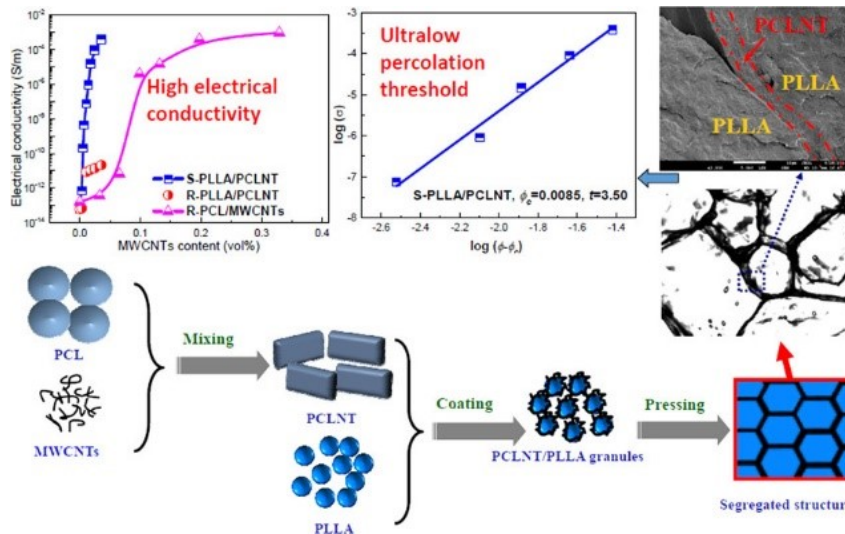

Figure 15 Comparison of electrical conductivity in the segregated S-PLLA/PCL/MWCNT, directly mixed R-PCL/MWCNTs, and directly mixed R-PLLA/PCLNT composites as a function of MWCNTs content. The inset shows the fitting lines for the R-PCL/MWCNTs composites by classical percolation theory processing procedure for preparing the PLLA/PCLNT composites with a segregated structure. Reprinted with permission from Shi et al[83]. Copyright 2017 American Chemical Society.

Table 3 Selective localisation of nano-sized fillers polymer composites having co-continuous morphology

Blend	Ratio	Filler	Composite preparation method	Percolation threshold (filler to whole resin)	Electrical conductivity S/cm	Phase selection	Refs
PET/PVDF	50:50 vol%	CNT 6 vol% mix with PET	Compounding	-	0.059 @ 6 vol% CNT mixed with PET	PET	[84]
PP-PS	70:30 vol%	CB 1 vol.% SBS 5 vol.%	Melt compounding	1.55 wt%	0.5 @ 1 vol% CB	SBS	[74]
PMMA-PU	75:25, 80:20, 85:15 wt%	CB content (1~5 wt%)	Radical bulk polymerization	2 wt% of CB for PMMA/PU (80:20) and (85:15); 3 wt% of CB for PMMA/PU (75:25)	2.05×10^{-6} @ 5 wt% CB for PMMA/PU (80:20)	-	[85]
LDPE-PVDF	2:1, 1:1 vol%	MWCNT	Melt compounding	5.7 vol% for PVDF- LDPE ratio 2:1; 7.1 vol% for PVDF-LDPE ratio 1:1	1×10^{-6} @8 vol% MWCNT for PVDF-LDPE (2:1)	LDPE	[86]
HDPE-UHMWPE	25:75 & 50:50 wt%	Carbon fiber 15 wt.% Graphite 60 wt.%	Dry mix, Hot press		69 @15 wt% CF + 60 wt% Graphite for HDPE-UHMWPE (25:75)	HDPE	[87]
HDPE-PMMA	20:80-80:20 wt%	CB 30 phr (in HDPE)	Two roll mill		1×10^{-2} @ 30phr CB for HDPE-PMMA(80:20)	HDPE	[88]
PMMA-PP	20:80-60:40 wt%	CB 10 Phr (in PMMA)	Two roll mill		1×10^{-4} @ 10Phr CB for PMMA-PP (40:60)	PP	[88]
PC-PS	50:50 vol%	CNT 0.05 -5 wt%	Solution compounding	0. 5 wt%	0.77 @5wt% CNT for PC-PS (50:50)	PS	[89]
PP-Novolac	90:10-40:60 wt%	CB 6 wt%	Melt mixing	CB 8phr in PP-Novolac 70/30	≈0.1 @ 17phr CB for PP/Novolac (70:30)	PP	[90]
LCP-PC	20:80 wt %	CNT 0.5-15 wt%	Melt mixing	1 wt % CNT	1×10^{-2} @ 15 wt% CNT for LCP-PC (20:80)	LCP	[91]
PET-PE	1:3.2 vol%	CB	Melt mixing	3.8 vol% CB	1×10^{-3} @ 12 vol% CB for PET-PE (1:3.2)	PET	[92]
PA6- PP	10:90-30:70 wt%	CB	Melt mixing and compression molding		0.0067 @ 6 wt% CB for PA6-PP (20:80)	Interface PA6-PP	[93]
PET-PVDF	50/50 wt%	CF-10phr CNT-5phr	Melt mixing		0.1 @ 10 phr CF + 5 phr CNT for PET-PVDF (50:50)	PET	[94]
PE-PP	60:40-40:60 wt%	MWCNT	Melt mixing	1.3 wt% MWNT	0.05 @ 7 wt% MWCNT for PE-PP (60:40)	PE	[95]
HDPE-iPP	50:50 wt%	VGCF 2.5phr	Two roll mill	1.25 phr VGCF	1×10^{-4} @ 2.5 phr VGCF for HDPE-iPP (50:50)	HDPE	[96]

UHMWPE-HDPE	97:2.7 wt%	UHMWPE-HDPE	Solution blending	0.3 wt%	8.4×10^{-7} @ 0.3wt% CNT for UHMWPE-HDPE (97:2.7)	HDPE	[97]
PS/PMMA	50:50 vol%	PS/PMMA	Melt mixing	1 vol%	10^{-3} @ 10 vol% CB for PS/PMMA (50:50)	PS	[98]
PA6/ABS	60/40-40/60 wt%	PA6/ABS	Melt mixing		10^{-5} @ 5 wt% MWNTs for PA6/ABS (60:40)	PA6	[99]
PP/POE	70:30 wt%	CNT	Melt compounding	4 wt.%	5×10^{-8} @ 10 wt% CNTS for PP/POE (60:30)	PP	[100]
PP/UHMWPE	70:30 wt%	CNT	Melt compounding	2.8 wt.%	5×10^{-5} @ 10 wt% CNT for PP/UHMWPE (60:30)	PP	
PP/POE-g-MA	70:30 wt%	CNT	Melt compounding	4.5 wt%	5×10^{-12} @ 10 wt% CNT for PP/POE-g-MA (60:30)	PP	
PLLA / PCL	95:5 wt%	MWCNT	Melt mixing	0.012 wt%	3.84×10^{-6} @ 0.05 wt% MWCNT for PLLA/PCL (95:5)	PLLA	[101]
PP/HDPE	80:20 wt%	CF	Melt mixing		2.5×10^{-4} @ 5wt% CF for PP/HDPE (80:20)	PP	[102]
PDMS/PANI	95:5 wt%	CNT	Ultrasonic treatment		3.4×10^{-4} @ 2 wt% CNT for PDMS/PANI (95:5)	PDMS	[103]
CPA/PP	84:12.5 vol%	CNT	Melt mixing		5×10^{-7} @3.5wt% CNT for CPA/PP (84:12.5)	CPA	[104]
PP/CPA	84:12.5 vol%	CNT	Melt mixing		10^{-6} @ 2.5 wt% CNT for PP/CPA (84:12.5)	PP	
PMMA/LDPE	80:20 wt%	MWCNT	Melt compounding	2 wt%	10^{-2} @ 5 wt% MWCNT for PMMA/LDPE (80:20)	LDPE	[105]
LDPE/PMMA	80:20 wt%	MWCNT	Melt compounding	3.5 wt%	10^{-3} @ 5 wt% MWCNT for LDPE/PMMA (80:20)	LDPE	

2.3.3 Segregated structures

Segregated structures can be created by compression-moulding a mixture of polymer granules coated with conductive fillers through dry or solution mixing, or by selective distribution of fillers at the interfaces of immiscible polymer blends through melt-compounding. The segregated conductive network leads to an ultra-low φ_c in the range of 0.005~0.1 vol%, high electrical conductivity of up to 10^6 S/m, and good EMI shielding effectiveness (above 20 dB) at low filler loadings[106].

MWCNTs were initially mixed with PCL, then coated onto PLA particles at 100 ºC, a temperature between the melt temperatures of PCL and PLA, as shown in Figure 15. A following compression moulding at above the melt temperature of PLA generated segregated PCL/MWCNT structures. The MWCNTs were selectively dispersed in the PCL phase, resulting in a low φ_c of 0.0085 vol%. A high electrical conductivity of 3.84×10^{-4} S/m was obtained at 0.05 wt% of MWCNTs[83].

Poly(ethylene-co-octene) (POE)/MWCNT elastomeric composite was prepared by mixing MWCNTs with chemically cross-linked POE granules to form a segregated structure, as shown in Figure 16b. The percolation threshold of 1.5 vol% was observed, much lower than that of the melt-mixed POE/MWCNT composites, 9 vol%, see Figure 16a. This was associated with the denser conductive network formed in the selective POE phase[107].
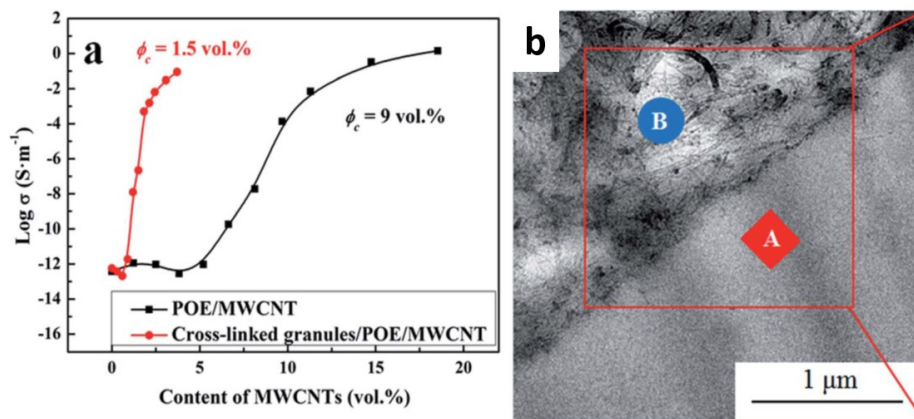
Figure 16 (a) Electrical conductivity as a function of MWCNT content and (b) TEM images of cross-linked granules/POE/MWCNT-3.7. Reprinted with permission from Li et al[107]. Copyright 2015 Royal Society of Chemistry.

From the above discussion, it is clear that the structure and morphology of multiphase composites directly determine the electrical properties. A recent study compared the electrical conductivity and EMI performance of PE/CNTs composites with different structures, segregated (s-CNT/PE), partially segregated (p-CNT/PE) and randomly distributed (r-CNT/PE)[108]. The percolation threshold values were calculated to be 0.013, 0.025, and 0.310 vol% for s-CNT/PE, p-CNT/PE and r-CNT/PE, respectively. With 0.8 wt% of CNTs, the s-CNT/PE composite exhibited electrical conductivity of 0.89 S/m, about 47 and 182 times higher than that of the p-CNT/PE and r-CNT/PE composites respectively. Over the frequency range of 8.2–12.4 GHz (X-band), with the same CNT concentration of 5 wt%, the s-CNT/PE composite achieves an EMI shielding effectiveness (SE) as high as 46.4 dB, which was 20% and 46% higher than the p-CNT/PE and r-CNT/PE composites, respectively. The segregated s-CNT/PE composite with highly dense CNT networks contributes to the increased electrical conductivity as shown in Figure 17 (a-b). With only 1.0 wt% CNT addition, an EMI SE of 20.8 dB was achieved at the frequency of 12.4 GHz. This can be associated with the numerous interfaces that absorb electromagnetic waves, and demonstrates

the effectiveness of improving EM performance by tailoring the morphology and structures of the composites, see Figure 17 (c-d).
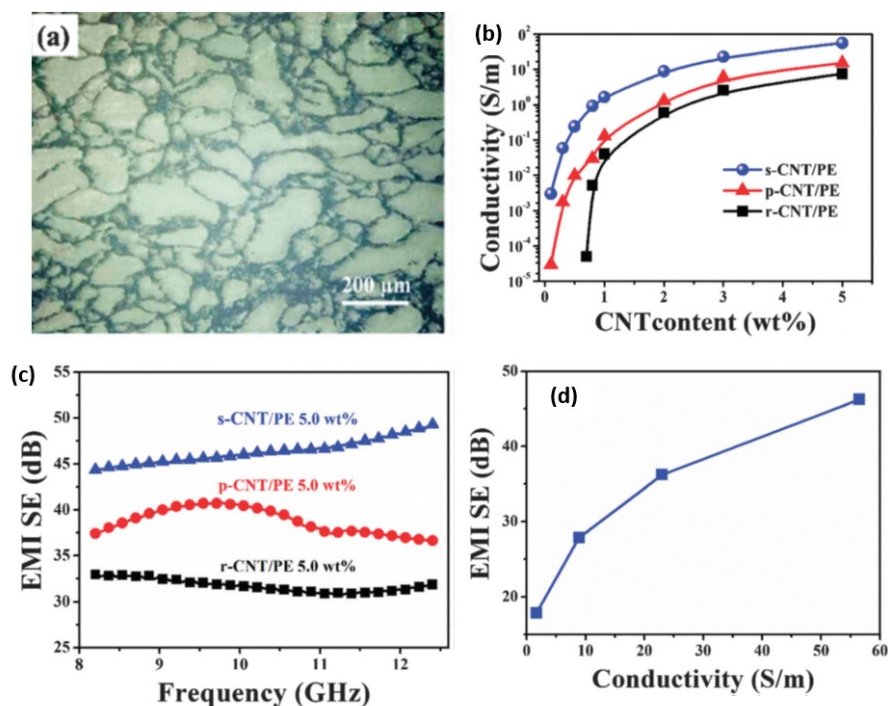

Figure 17 SEM images of (a) s-CNT/PE composites; (b) electrical conductivity and (c) EMI SE of the three CNT/PE composites with 5.0 wt% CNTs in the X-band frequency range, (d) The average EMI SE as a function of electrical conductivity of the s-CNT/PE composite. Reprinted with permission from Jai et al[108]. Copyright 2015 Royal Society of Chemistry.

2.4 Selective localisation of hybrid fillers in polymer blends

Selective distribution of multiple nanofillers in different phases of polymer blends has provided additional opportunities to tune the morphologies and functionalities of polymer composites.

To obtain a high shielding effectiveness (SE) in polymer based systems without using metallic shields, the combination of conducting carbonaceous nanomaterials and metallic particles have been an effective strategy to create lightweight EM shielding materials[109]. The electrically conductive CNTs or graphene contribute to the reflection mechanism of EM waves due to their high aspect ratio and skin effects[110]; while the metal/metal salts provide

magnetic and dielectric properties and act as EM absorbers to convert the EM energy into thermal energy and dissipate it through the surface[111]. In this type of composite, the combination of carbon and metal particles provides both conductivity and magneto-dielectric loss to the composites. The shielding effectiveness depends on the filler type, their dispersion and location, polymer-filler interfaces as well as the configuration of the products[112].

2.4.1 Metal-filled polymer composites

Metallic particles filled polymer composites exhibit a number of advantages over metals such as flexibility, lightweight, corrosion resistance, together with the ability to form complex parts due to the ease of processing of polymers. The electrical, thermal conductivity and mechanical properties of polymers have been improved by adding metal particles such as aluminium, nickel, copper, iron and silver [113], examples are shown in Table 4.

However, the large difference in surface energy between metal particles and polymers result in poor interfacial adhesion[114]. The wide distribution of the shape, size and properties of metal particles result in a percolation threshold in the range of 8 and 40 wt%, such high loading of metallic particles inevitably deteriorate the mechanical and processing properties of the polymers. Despite their universal importance in numerous applications, such as EMI shielding, passive components as heat sinks in electronic circuits and pressure sensors, metal-filled plastic composites have not been systematically studied [115].

By using LDPE as a matrix, the addition of copper particles with size of 38 μm reached an electrical percolation threshold at 19 vol%[116]. In comparison, the addition of smaller copper particles (0.2-0.3 μm) could reduce the percolation threshold to 10 vol% [117]. High aspect ratio metal particles are preferable to form a conductive network at low concentration levels. Copper nanowires filled SBS [118] composites displayed a high conductivity of 1858 S/cm, and a high elongation at break of 920%. In addition, the electrical performance of the

composite was not affected after deformation to a bending radius of 4.0mm for 1000 cycles. It was important that the copper nanowire filled SBS composites could be directly printed onto paper to produce flexible circuits with excellent electrical performances under different tension conditions.

For branch-structured nickel particles filled LDPE[119], a maximum electrical conductivity was achieved at 83 S/cm and a thermal conductivity of 1.99 W/mK, but at a filler concentration as high as 30 vol%. An electrical percolation threshold was identified at 8 vol%. Processing PVDF/nickel composites by solution mixing resulted in a percolation threshold of 16 vol% [120]. In comparison, a higher percolation threshold of 28 vol% was observed for PVDF/nickel composites when prepared by dry mixing and hot pressing [121].

2.4.2 Selective location of hybrid metal-carbon particles in polymer composites

The EMI shielding performance of polymer composites relies on multi-component and multi-phase design. Some of the latest developments are summarised in Table 5.

The doping of α-MnO$_2$ onto MWCNTs ensured intrinsic wave impedance matching in addition to providing conducting pathways, and the ferrite-doped cross-linked GO facilitated the enhanced attenuation of the incoming EM radiation. When both types of hybrid fillers were added to a binary immiscible co-continuous PC/PVDF (50/50 wt%) blend, the filler particles were selectively located in the PVDF phase due to a polarity mismatch. This magneto-dielectric coupling led to a high electromagnetic shielding efficiency (SE) of -37 dB at 18 GHz, dominated by absorption-driven shielding. A multilayer structure by stacking individual composites was able to form an absorption–multiple reflection–absorption pathway, and resulted in an SE of -57 dB for a thin shielding layer of 0.9 mm thickness. Such a high SE indicates >99.999% attenuation of the incoming EM radiation[122].

MWCNT was doped with flower-like Fe_3O_4 nanoclusters, then added to PC/PVDF (50/50 wt%) blends to form composites. The hybrid Fe_3O_4/MWCNT filler dissipated heat effectively. Stacking the composites in a specific sequence resulted in a high shielding efficiency of −64 dB at 18 GHz for a shield thickness of 0.9 mm[123]. The hybrid Fe_3O_4/MWCNTs fillers provided absorption driven shielding due to the presence of both electrical and magnetic dipoles, together with multiple interfaces.

To improve the interface adhesion of co-continuous immiscible polymer blends, a third polymer PMMA (10 wt%) was incorporated into the immiscible PVDF/PC (40/60 wt%) blends due to its mutual compatibility with both PVDF and PC. The electrical conductivity was enhanced by selectively locating ionic liquid modified MWCNTs in the PVDF phase and the magnetic properties were tuned by locating BaFe nanoparticles in the PC phase via a nucleophilic substitution reaction, see Figure 18. Thus, the conducting MWCNTs surface reflected back incident EM radiation by approximately 40%. The incoming radiation suffers multiple scattering within the CNT network and the penetrated EM radiation was also absorbed by the BaFe nanoparticles, accounting for the absorption of 60% of the microwave radiation. The PMMA acted as an interfacial modifier in the PC/PVDF blends for a significant enhancement in mechanical properties, in addition to retaining high shielding effectiveness (SE) of -37 dB at 18 GHz frequency[124].
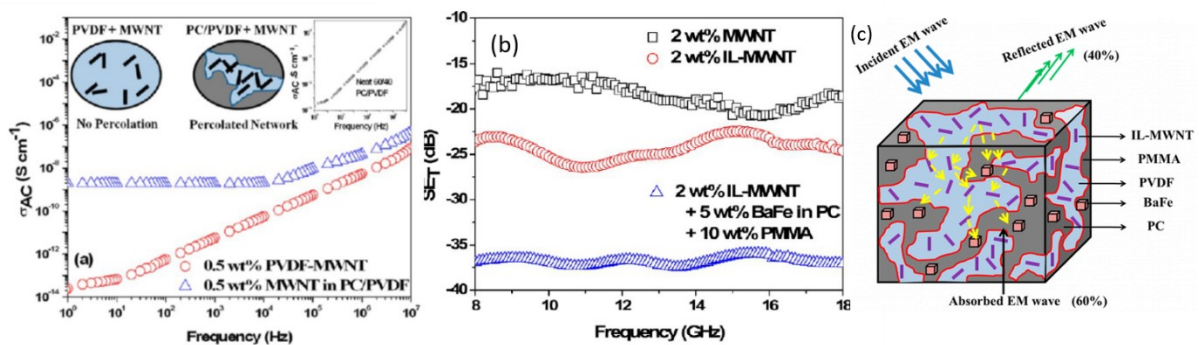
Figure 18 (a) AC electrical conductivity of PVDF/MWCNT and 60/40 PC/PVDF/MWCNT composites; (b) total shielding effectiveness (SE$_T$) of these composites; and (c) the mechanism of EM attenuation for blends containing 2 wt% IL-MWNT in PVDF phase and 5 wt% BaFe in the PC phase. Reprinted with permission from Biswas et al[124]. Copyright 2015 American Chemical Society.

Table 5 EMI shielding performance of multi-component and multi-phase composites

Polymer	Nanoparticles	Frequency (GHz)	Thickness (mm)	SE$_{total}$ (dB)	Refs
PVDF	MWCNT 5 wt%	18-26.5	0.1	22.41	[52]
	Graphene 10 wt%	18-26.5	0.1	18.7	[52]
	MWCNT 5 wt% + graphene 10 wt%	18-26.5	0.1	27.58	[52]
	Graphene + graphene quantum dots (2 wt%)	12		37	[125]
	Graphene + graphene quantum dots (2 wt%)+Ag	12		46	[125]
	rGO –Co$_3$O$_4$ (10 wt%)	2-18 (11.6)	4		[126]
	rGO –MnFe$_2$O$_4$ (5 wt%)	2-18 (9.2)	3	-29	[127]
	rGO –MnFe$_2$O$_4$ (5 wt%)+ MWCNT (3 wt%)	2-18 (18)	3	-38	[128]
	rGO –FeCo (10 wt%)+ MWCNT (3 wt%)	8-18 (12)		-41.2	[129]
	rGO-MoS$_2$ (5 wt%)	2-18 (14.48)	5	-27.9 (25 wt%)	[130]
	3D crosslinked rGO –FeCo (10 wt%) + MWCNT (3 wt%)	12-18	5	-41	[129]
PS	carbide/carbonitride (MXene) (1.90 vol%)	8.2-12.4	2	-62	[131]
PC/SAN (60/40 wt%)	rGO-Co/MWCNT(10 wt% +3 wt%) in PC phase	12-18 (18)	5	-34	[132]
PVDF/PC (40/60 wt%) + PMMA (10 wt%)	IL-MWCNT (2 wt%) + BaFe (5 wt%)	2-18 (18)	1	-37	[124]
PVDF/PC (50/50 wt%)	rGO -Fe (5 wt%)+ MWCNT/α-MnO$_2$ (3 wt%)	8-18(18)	0.9	-37	[122]
	MWCNT 3 wt% + Fe$_3$O$_4$ 3 wt% Three layer assembly	18	0.9 0.9	-32 -64	[123]

2.5 Electrical conduction mechanism of polymer composites

Table 6 Prediction models of conductive composites

Model	Mechanism / assumption	Conductivity prediction formula	Applicability
Classical model	Based on the dimension of	$\sigma = \sigma_0(\varphi - \varphi_c)^t$	More suitable for an

	network geometry	t is an index related to the dimension of the conducting network. For 2D network, t ≈ 1.3; for 3D network, t ≈ 2.0.	approximate trend forecast
Voetmodel [133]	Non-Newtonian conduction mechanism. Particle transmission and electron emission.	$log\sigma = K\varphi^{\frac{1}{3}}$, K is a constant	Considering the action of electron emission mechanism for filler content below percolation threshold
Electron Tunneling Effect model[134]	Based on simple tunnel conduction model	$$\sigma_{dc} = \sigma_0 e^{-2X_t d}$$ σ_c is the resistivity of the conductive filler, d is the tunnelling gap between conductive particle, X_t is the gap barrier coefficient	Occurs when the distance between conductive particles is close, about 10 nm
Scarisbrick model[135]	Conductive network formed through particle contact. The particle is in Ohmic contact. The particles are spherical in random distribution	$$\frac{\sigma_c}{\sigma_f} = \varphi \times \varphi e^{(V_c)-2/3} \times C^2$$ σ_c is the electrical conductivity of composites; σ_f is the electrical conductivity of filler; c is geometric parameter; φ_c is the volume fraction of conducting filler in the composite	Statistical model suitable for EVA/CB and EVA/SCF of high filler content, not suitable for EVA/MWCNT
McCullough model[136]	Based on transport mechanism	$$\sigma_c = \varphi_p\sigma_p + \varphi_f\sigma_f - \left(\frac{\varphi_p\varphi_f\lambda(\sigma_f-\sigma_p)^2}{V_f\sigma_f + V_p\sigma_p}\right)$$ σ_c is conductivity of the composite; σ_p is conductivity of pure polymer; σ_f is conductivity of filler (CB- 5,260 S/cm，MWCNT- 100 S/cm; λ is a structural factor related to the formation of conductive chains and networks (varying from 0 to 1)	Can predict the conductivities of homogeneous systems
Bueche model [137]	Based on aggregation of conductive particles that forms gel network in polymer matrix	$$\sigma_c = \varphi_f\sigma_f + (1 - \varphi_f)\sigma_p$$ φ_f is volume fraction of filler；σ_p is conductivity of polymer (10^{-10} S/cm)	Not suitable for multi-component system of which component has large difference in performance
Modified Scarisbrick model[138]	A modified Scarisbrick model by introducing filler aspect ratio,	$$\sigma_c = C \times \sigma_f \times \frac{A}{10} \times S \times \varphi \times (\varphi)^{\varphi^{-\frac{2}{3}}}$$ $$+ (1 - \varphi)\sigma_p$$	Suitable for both high and low content of EVA/CB,

	surface area to volume ratio and conductivity of the polymer matrix. Provides better agreement between experimental and theoretical conductivities	σ_c is conductivity of composites σ_p is conductivity of polymer；φ is volume fraction of filler；C is a geometric parameter defining geometry, arrangement and overlap over conductive chains in the polymer matrix	EVA/SCF and EVA/MWCNT

A variety of models have been developed to estimate the electrical conductivity upon the addition of fillers to an insulating polymeric system by taking into account different factors and properties, such as those listed in Table 6. For example, some of these models assume particle contact and thus only work once the percolation threshold has been reached. Others models, such as the Voet model[133], work below the percolation threshold to predict conductivities.

The Voet model was initially developed to estimate how the presence of carbon black affects the electrical conductivity. Carbon black has a low packing density under normal atmospheric conditions and a void density of up to 97%. The unique structural characteristics induce

electron tunnelling through the voids, rather than electron hopping or through particle contact[133]. Similarly, the Electron Tunnelling Effect (ETE) model [134] was designed to calculate the electrical conductivity of a material below the percolation threshold, assuming electron tunnelling is the dominant conduction pathway. This model is applicable for graphite filled systems, where the Voet model is not suitable because of the different structures between graphite particles and carbon black, where graphite has a well-developed crystalline structure, large particle size and a lower tendency to aggregate as compared to carbon black. In addition, the ETE model factors in the influence of temperature on lowering the energy barrier height for electron transmission；and the resulting influence on the electrical conductivity[134].

Unlike the aforementioned models, the McCullough model [136] is a generalised model to predict the transport properties of a composite. It takes into account a wide variety of factors such as filler shape and is able to calculate several different properties such as electrical conductivity, thermal conductivity,[1] dielectric constant, magnetic permeability and diffusion coefficients. This model also uses electron tunnelling as the conduction mechanism within the composite, and thus is unsuitable for calculations at or beyond the percolation threshold. Whilst most properties used in the models can be calculated experimentally, there are two properties, namely the effective chain property and structure factor that are difficult to calculate using this model.

In comparison, the Bueche model [137] assumes a different mode of transport in a composite system, in which the filler can be thought of as a series of infinite chains that are touching. This therefore means that the model is able to work above the percolation threshold. However, it deviates from experimentally observed results at low filler concentrations. This model makes a series of idealised assumptions. Firstly, it assumes that a lattice of identical spherical particles form, which are able to form a uniform packing structure. Secondly, the model assumes that a good dispersion of filler is present. Finally, this model is based on the rules of additivity, where the addition of the filler is assumed to have similar properties to the medium already present, e.g. similar conductivities. This means that when adding a conductive filler to an insulating medium, the model does less well in predicting properties.

Finally, the Scarisbrick model [135] assumes that conduction takes place via particles that are in contact. The model is based on the theory of a liquid structure, where the volume of filler particles is randomly distributed in the matrix and there is no long-range order in the system. The model is able to take into account particle size, shape, orientation, contact resistance and packing arrangements and the bulk material properties are an average of all of the individual

particles present in the composite. The approach works well for modelling how conducting carbon black and short carbon fibre composites behave. However, this model was later modified to include the aspect ratio of the filler and its surface area to volume ratio so that MWCNTs could be modelled more effectively[138].

Figure 19 shows how each of the models performed with regard an ethylene vinyl acetate (EVA) composite with MWCNTs. It can be seen that the McCullough and Bueche models are typically orders of magnitude out in predicting electrical conductivity. The Scarisbrick model is also incorrect at low MWCNT filler loadings. However, the model and the experimental results converge together, with the model also following the shape of the experimental curve. The modified Scarisbrick model is able to predict the conductivity of the composite much more closely, demonstrating an improved relationship between theoretical and experimentally determined values[138].
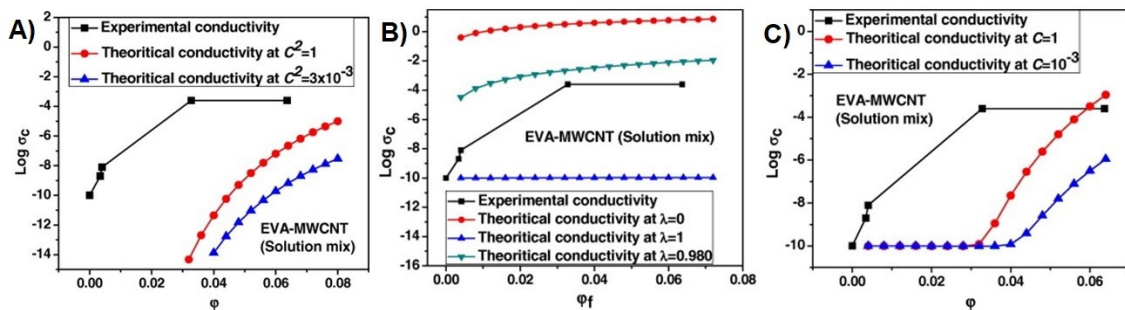
Figure 19 Graphs that show how A) the Scarisbrick model, B) the McCullough model and C) the modified Scarisbrick model performed at predicting the conductivity of EVA-MWCNT composites as a function of filler loading. Reprinted with permission from Sohi et al[138]. Copyright 2011 Elsevier.

Table 4 Percolation threshold (φ_c) of metal-filled polymer composites

Matrix	Metal powder	Particle size (μm)	Mixing method	φ_c (vol%)	Max. electrical conductivity S/cm	Refs
LDPE	Copper	38	Internal mixer	18.7	0.11 @ 24 vol% Copper + 76 vol% LDPE	[116]
LDPE	Copper	0.2-0.3	Mechanical mix	10	1 @35 vol% Copper + 65 vol % LDPE	[117]
HDPE	Aluminum	83.0	Internal mixer	45-55 wt%	1 @65 vol% aluminum + 35vol % LDPE	[139]
	Silver	9.0	Internal mixer	55-65 wt%	1000 @55 vol% silver + 45 vol% HDPE	
HDPE	Nickel		Melt mix	8		[140]
HDPE	Silver	0.15	Melt mix, twin screw	17	0.01 @24 vol% silver + 76 vol% HDPE	[141]
HDPE	Aluminum	25	Melt mix	35	10^{-2} @ 55 vol% Aluminum + 45 vol% HDPE	[142]
	Copper	36	Melt mix	--	conductance $10^{5.7}$S @ 55 vol% Copper + 45 vol % HDPE	
	Iron	9	Melt mix	--	conductance $10^{5.3}$ S @55 vol% iron + 45 vol% HDPE	
HDPE	Iron	50.0-100.0	Roll mill	12		[143]
PBT	Silver	0.15	Melt mix, twin screw	13	0.001 @24 vol% silver + 76 vol% PBT	[141]
Nylon (MXD6 [a])	Silver	0.15	Melt mix, twin screw	17.5	0.01 @ 24 vol% silver + 76 vol% Nylon	
CPA	Iron	2.0	Melt mix, twin screw	20	0.01 @ 38 vol% iron + 62vol% CPA	[144]
PE	Silver	0.1	Melt mix, twin screw	10	0.1 @ 22vol% silver + 78vol% PE	[145]
PVC	Nickel	100	Dry mix, hot press	4.0	$10^{2.5}$ @ 30 vol% nickel + 70 vol% PVC	[146]
	Copper	100	Dry mix, hot press	5.0	$10^{3.8}$ @ 38vol% copper + 62vol% PVC	[146]
EVA	Zinc		Dry mix	19	3.2×10^{-5} @ 75wt% of zinc+ 25wt. % EVA	[147]
Lignocellulose	Copper	45	Dry mix, hot press	11	10^{2}@(30vol. % copper + 70 vol% Lignocellulose	[148]
PVDF	Nickel	0.05	Solution blending	16	0.0014 @ 35 vol% nickel + 65 vol% PVDF	[120]
PVDF	Nickel	0.02	Dry mix, hot press	57	10^{-7} @ 57 vol% nickel + 43 vol% PVDF	[121]
PVDF	Silver	0.1	Solution blending	20		[149]
PS	Copper nanowire	0.025	Solution mixing, then dry mixing	0.24	100 @ 3 vol% Copper Nanowire+ 97 vol% PS	[150]
PS	Copper nanowire	0.025	Solution mixing	2.0	10^{-5} @ 4 vol% Copper Nanowire + 96 vol% PS)	[151]
PP	Iron	2.0	Melt mix, twin screw	24	0.01@ 38 vol% iron + 62 vol% PP	[144]
PPS	Copper	0.5-2.0	Mechanical mix	6	10^{-7}@ 20 vol% Copper + 80 vol% PPS	[152]
PEKK	Silver Nanowire	0.1-0.4	Melt mix	0.59	2@ 5 vol% Silver Nanowire+ 95 vol% PEKK	[153]
HDPE/PBT	Silver	0.15	Melt mix twin screw	8	10^{-2}@ 20 vol% silver + 80 vol% HDPE/PBT	[141]
HDPE/MXD	Silver	0.15	Melt mix, twin screw	10	10^{-2}@ 20 vol% silver + 80 vol% HDPE/MXD	[141]
PE/POM	Iron	3.5	Melt mix, twin screw	9	0.01@35 vol% iron+ 65 vol% PE/POM	[154]
PP/CPA	Iron	2.0	Melt mix, twin screw	5	0.01@ 35 vol% iron+ 65 vol% PP/CPA	[144]

Polymer	Filler		Method			Ref
PE	Iron	3.5	Melt mix, twin screw	21	0.01@40 vol% iron+ 60 vol% PE	[154]
POM	Iron	3.5	Melt mix, twin screw	24	0.01@40 vol% iron+ 60 vol% POM	[154]
Polyaniline	Silver		In situ deposition	16.2	10000@40 vol% Silver+ 60 vol% Polyaniline	[155]
PVC	Copper	44	Hot press	20 wt%	40@40 vol% copper+ 60 vol% PVC	[156]
PMMA	Aluminium	63	Solution cast	20 wt%		[157]
PVDF	Nickel		Solution mix	27.2	0.002@34 vol% nickel+ 66 vol% PVDF	[158]
	Tungsten		Solution mix	34.4	5×10^{-6}@45 vol% tungsten+ 55 vol% PVDF	[158]
	Zinc		Solution mix	31.8	5×10^{-4}@50 vol% zinc+ 50 vol% PVDF	[158]
SBS	Copper nanowires		Vacuum filtrated		1858@20 wt% CUNWS+ 80 wt% SBS	[118]
PANI	Silver		In-situ polymerization		6.6×10^{-2} @ temperature of 433K	[159]
PS	Silver		In-situ bulk polymerization		103@20wt% silver+ 80 wt% PS	[160]
PMMA	Silver		In-situ bulk polymerization		33@20wt% silver+ 80 wt% PMMA	[160]
PS/PMMA	Silver		In-situ bulk polymerization		40×10^{-3}@20wt% silver + 80wt% PS/PMMA	[160]

Table 7 Properties of polymer/metal composites

Filler/matrix systems	Filler concentration	Thermal conductivity of filler (W/mK)	Thermal conductivity of composite (W/mK)	Mixing method
Ag/ PVDF[161]	Ag, 20 vol%	420	6.5	Melt mixing
Ag/MWCNT/HDPE[162]	0.2 wt% MWCNT+ 3 wt% Ag	420	0.714	Melt mixing
Ag/PI[163]	--	420	27	Electro- spinning
Ag/PA/PE[164]	Ag coated PA, 33.4 vol%	420	1.935	
Cu/ PS microsphere[165]	Cu, 23 vol %	377	26.14	Hot embossing
Al/PVDF[166]	Al, 50 vol%	270	3.258	Rheometer at 180 °C and 20 min, then hot embossing
BN/MWCNT/PPS[167]	50 wt% BN + 1 wt% MWCNT	250, 2800	1.74	Melt mixing
h-BN$_{60}$/h-BN$_{110}$/PPS[168]	25 vol% h-BN$_{60}$ + 8.3 vol% h-BN$_{110}$	300, 300	2.04	Melt mixing
h-BN$_{60}$/MWCNT/PPS[168]	25 vol% h-BN$_{60}$ + 8.3 vol% MWCNT	300, 3000	2.16	Melt mixing
Graphite/CF/PA6[169]	30 wt% graphite + 30 wt% CF	800, 500	5.09	Melt mixing
Al$_3$/Al$_{13}$/polyacrylate[170]	45 wt% Al$_3$ + 45 wt% Al$_{13}$	-	4.23	Ball milling followed by solution casting
Al$_3$/Al$_{13}$/MWCNT/polyacrylate[170]	45 wt% Al$_3$ + 45 wt% Al$_{13}$ + 1 wt% MWCNT	-	3.86	Ball milling followed by solution casting
AlN$_{10}$/Al$_2$O$_{3(0.5)}$/(ETDS-DDM) epoxy[171]	40.88 vol% AlN$_{10}$ + 17.52 vol% Al$_2$O$_{3(0.5)}$	285, 30	3.402	Solution blending and casting
1 μm h-BN/70 nm h-BN/PI[172]	21 wt% 1 μm h-BN + 9 wt% 70 nm h-BN	-	1.2	Solution blending and casting
AlN/MWCNTs/PGMA[173]	25 vol% AlN + 1 vol% MWCNTs	-	1.21	Solvent blending and casting
BN/T-ZnO/PF[174]	30 wt% BN + 30 wt% T-ZnO	400, 60	1.96	Solution blending and casting
SiC/GNP/DGEBA[175]	53 wt% SiC + wt% GNP	-	7.3	Solution blending and casting
h-BN/c-BN/Epon8008[176]	8.8 vol% h-BN$_{0.2}$ + 8.8 vol% h-BN$_{0.4}$ + 8.8 vol% c-BN	-	19.0	3 roll miller and casting
BN/single layer graphene/Epon8008[177]	10 vol% BN + 0.1 vol% single layer graphene	-	21.6	Solution blending and casting
SiC/MWCNTs/DGEBA[178]	15 vol% SiC + 15 vol% MWNCTs	120, 2000	2.1	Solution blending and casting
AlN/BN/DGEBA[179]	40 vol% AlN + 40 vol% Bn	-	8.0	Mechanical mixing and molded

3 Thermal conductivity of polymer composites

Polymers have low thermal conductivity in the range of 0.1~0.4 W/mK, the modification or

increase of the thermal conductivity of polymers is technically challenging. Metal particles and 1D and 2D carbon nanomaterials (6-6000 W/mK)[167] are promising for improving the thermal conductivity of polymers [180, 181], however interfacial defects between the fillers and polymer matrices can cause phonon scattering and lower the thermal conductivity (0.1-0.5 WmK)[182, 183]. Some examples are listed in Table 7. The effects of morphology, structure, dispersion, interface and processing on thermal conductivity of polymer composites have been comprehensively overviewed in our recent reviews [180, 181], here we will briefly discuss the thermal conductivity of hybrid filler systems on thermoplastics and thermosets, and pay particular attention on the theoretical modelling [184] of thermal conductivity of polymer composites, as summarized in Table 8.

3.1 Thermoplastic composites

Hybrid filler combinations have been introduced to combine fillers of different shape, size and composition to enable the formations of a hierarchical thermally conductive pathway, which overcomes the high concentrations of agglomeration of single filler systems, poor processability, decreased mechanical properties and high cost[168] [170]. Some examples of thermoplastic hybrid composites are given in Table 7.

Boron Nitride (BN) particles of different size and shape were incorporated together in PPS. The larger sized BN platelets act as a bridge between the smaller BN platelets when used in a 1:3 ratio in PPS. This increased the thermal conductivity to 2.04 W/mK. Replacing the larger BN platelets with MWCNTs aided a further improvement of the thermal conductivity to 2.16 W/mK. In this work, the size and shape of the MWCNTs as a secondary filler was deemed to aid phonon conduction between the small BN platelets[168].

The impact of fillers within a polymer matrix is hindered by weak interfacial bonding between the two phases[185]. This causes a high thermal resistance between MWCNTs and the polymer

matrix and as well as an inherently high contact resistance between MWCNTs and BN. Chemical modification of MWCNTs using hydrogen peroxide introduced hydroxyl groups onto the surface of the MWCNTs and improved the interfacial interactions. When mixed with BN and PPS, the modified MWCNTs demonstrated an improved thermal conductivity to 1.74 W/mK from 1.45 W/mK for unmodified MWNCTs[167].

Polyacrylate composites containing 45 wt% of 3 μm Al spheres and 45 wt% of 13 μm Al spheres showed an increase in thermal conductivity 4.23 W/mK. This is larger than the inclusion of 90 wt% of 3 μm Al spheres (2.57 W/mK) and 13 μm Al spheres (4.06 W/mK) due to the better packing of particles in the composite. The addition of 1 wt% of MWCNTs reduced the thermal conductivity to 3.86 W/mK due to the poor interfacial interactions between MWCNTs and polyacrylate preventing the MWCNTs from being monodispersed and aiding phonon conduction[170].

3.2 Thermoset composites

Thermoset polymer composites differ from thermoplastic polymer composites in that they result in a crosslinked polymer network after curing. From Table 7, thermoset polymer hybrid composites have led to significant increases in thermal conductivity, up to 21.6 W/mK [177]. Nonetheless, the combination of BN with metallic aluminium nitride (AlN) filler resulted in an increase in thermal conductivity to 8.0 W/mK. This was attributed to the high packing efficiency in the polymer composite which lowered the interfacial thermal resistance due to an optimised contact area between fillers.[179]

To reduce interfacial thermal resistance between MWCNTs and SiC, both were surface modified by grafting triethylenetetramine. This hybrid system lowered the viscosity of the composite, reducing agglomerations of MWCNTs to ensure a higher monodispersity. In addition, chemical modification of the fillers led to the formation of MWCNT-MWCNT conducting networks and SiC-SiC conducting networks with a lower interfacial thermal

resistance between the filler particles. As a result, the thermal conductivity improved from 1.6 W/mK for a single filler network to 2.0 W/mK for the hybrid network. Interestingly, increasing the filler content above 20 vol% led to increases in the thermal conductivity for the hybrid composite but a decrease was seen in the single filler networks.[178]

One example of thermoset hybrid polymer composites utilises single layer graphene sheets (0.1 vol%) with only 10 vol% of BN. Raman spectroscopy showed that when the graphene had no 'D peak' in their spectra, the thermal conductivity of the hybrid composite was 21.6 W/mK. This missing peak demonstrated that the graphene had an almost perfect structure with zig-zag type sample edges instead of armchair type.[177]

The interactions of BN can be tailored to form a network resulting in a thermal conductivity of thermoset composites up to 19.0 W/mK. This was achieved using 26.5 vol% of BN filler, with a 1:1:1 ratio of 0.4 μm sized h-BN, 0.2μm h-BN and 1 μm c-BN. The difference between h-BN and c-BN is that h-BN has an analogous crystal structure to graphite, whilst c-BN has a structural behaviour analogous to diamond[181]. This led to a high inter-filler contact area between the two types of BN which reduced interfacial thermal resistance and enhanced thermal conductivity[176].

3.3 Thermal conductivity modelling

Early models such as the Maxwell-Eucken model [186] considered the effective thermal conductivity of the continuous and discontinuous phase and the volume concentrations of the filler alongside a shape factor. However, this shape factor did not take into account the size, shape or spatial arrangement of the filler but only the volume occupied. The model provided good agreement at low spherical filler concentrations, where the filler particles are far apart and do not interact with one another. The model was later modified by Fricke to include homogeneous ellipsoidal particles[187] as well as cylindrical and flat plate filler geometries by Hasselman-Johnson-Benvensite[188]. From this work, the dispersion of the fillers was

found to be key for accurate correlation between experimentally and theoretically determined values for thermal conductivity. A generalised form of the model was developed by Hamilton and Crosser, which could be used for different particle shapes[189]. However, all of these models assume that all of the filler particles are homogenous and are not agglomerated or form networks. As a result, the models tend to deviate from experimentally observed results upon reaching the percolation threshold.

Bruggeman developed a model similar to that of Maxwell-Eucken but with different assumptions made about how permeability and field strength affect the properties of the composite. Once again, this model was only applicable for dilute concentrations of spherical fillers but was shown to work independently of the polymer used in the composite system[190]. The theory of the Bruggeman model was used by Every-Tzou-Hassleman to determine the effect of particle size of conducting diamond on the thermal conductivity of zinc sulphide particles. From this, they determined the link between the microstructure of the filler and the effect observed on the thermal conductivity. Large particles enhance the thermal conductivity in a composite whereas filler particles smaller than the Kapitza radius lower the thermal conductivity. This is because the interfacial thermal barrier increases as the particle size decreases, due to a larger thermal insulating coating layer. Their modified Bruggeman model was able to follow the observed thermal conductivity trends for particle fillers above the Kapitza radius[191].

Unlike the Maxwell-Eucken model, the Bruggeman model works well across the entire range of filler concentrations. However, neither of the aforementioned Bruggemen models factored in the shape of the filler on thermal conduction. Jaijun modified the original Bruggeman equation so that both the filler shape and size were factored in. This resulted in a model that was in better agreement with experimental data than the original model (Figure 20)[192].
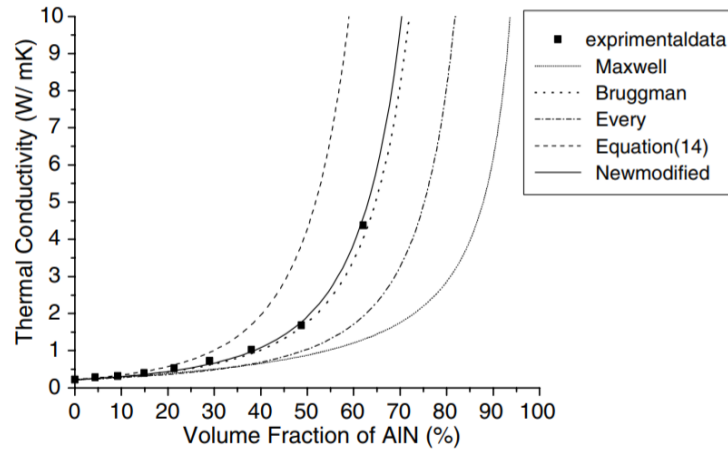
Figure 20 Variation in thermal conductivity with increasing content of aluminium nitride powder experimentally and compared to prediction from several models including the Maxwell model, Bruggeman model and Jaijun model (referred to as 'Newmodified'). Reprinted with permission from Jiajun et al[192]. Copyright 2004 Elsevier.

Agari developed a model using a generalisation of parallel and series conduction modes for composite systems, which was further modified by assuming that the dispersion of the filler is isotropic[193]. In parallel conduction modes, the conducting filler is arranged parallel to the direction of thermal flux, which results in the highest thermal conductivity. Conversely, in series conduction modes the conducting filler is arranged in series to the direction of thermal flux, as shown in Figure 21.
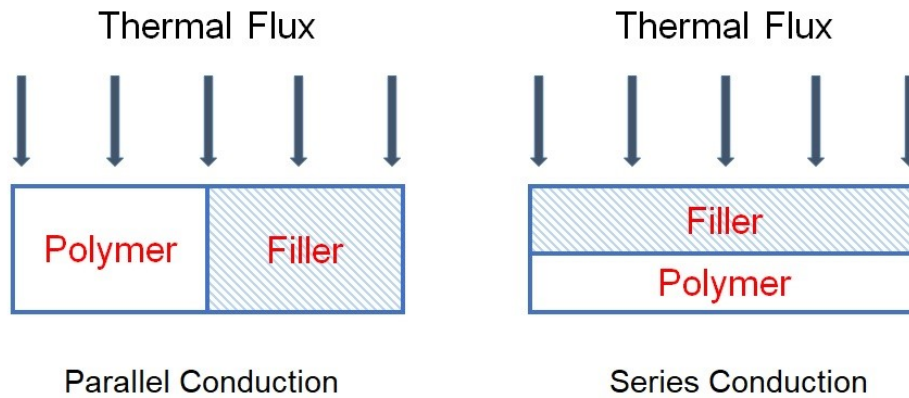
Figure 21 Conduction modes of thermal flux in: A) parallel conduction and B) series conduction in a composite material. Adapted with permission from Agari et al[193]. Copyright 1986 John Wiley and Sons.

This model works well for filler contents up to 30 vol%. However, it requires two experimentally determined values: 1) a factor for the ease of forming conductive chains and 2) a factor accounting for the crystalline content/crystallite size of the polymer which impact on the thermal conductivity of the composite. In later work, the extent of filler dispersion was incorporated into the model to account for poorer dispersions and agglomerations from different processing techniques such as in roll-milled mixing and melt mixing[194].

Table 8 Theoretical models for thermal conductivity of composites

Thermal conduction model	Equation	Characteristic
Maxwell-Eucken model[186]	$$Kc = \frac{2K_m + K_f + 2\emptyset_f\ (K_f - 2K_m)}{2K_m + K_f - 2\emptyset_f\ (K_f - 2K_m)} K_m$$	Maxwell-Eucken model predicted that the filler particles are uniformly distributed in the matrix, there is no interaction between particles and the shape of the particles is spherical and randomly distributed. But the model is only suitable for low filler contents Kc—Thermal conductivity of polymer composites； K_m—Thermal conductivity of polymer matrix materials； K_f—Thermal conductivity of the filler $\emptyset_f$—Volume fraction of filler in composite materials；
Bruggeman model[190]	$$(1 - \emptyset_f)^3 = \frac{K_m}{K_c}\left(\frac{K_c - K_f}{K_m - K_f}\right)^3$$	Bruggeman proposed that the interaction of neighboring particles can be equivalent to the increasing of the number of dispersed particles in the calculation of thermal conductivity of composites with high filler content.
Russell model [195]	$$K_c = K_m\left[\frac{\phi_f{}^{2/3} + \frac{K_m}{K_f}(1 - \phi_f{}^{2/3})}{\phi_f{}^{2/3} - \phi_f + \frac{K_m}{K_f}(1 - \phi_f{}^{2/3})}\right]$$	Russell model is based on the similarity between heat conduction and electrical conduction. Assuming that the filler is of the same geometry, no interaction and evenly distributed in the polymer matrix in the cube.
Fricke model [187]	$$K_c = K_c\frac{1 + V\left[F\left(K_f/K_m - 1\right)\right]}{1 + V(F - 1)}$$ Where $F = \frac{1}{3}\sum_{i=1}^{3}\left[1 + \left(K_f/K_m - 1\right)f_i\right]^{-1}$ $\sum_{i=1}^{3}f_i = 1$，$f_i$refers to the length of the semi axis of elliptical particles。	Fricke assumes that the filler particles are elliptical and randomly distributed in the continuous matrix. When f1=f2=f3, the filler is spherical and the Maxwell equation applies. When f1=f2≠f3, the particle is an ellipsoid.

Model	Equation	Description
Hamilton and Crosser model [189]	$$Kc = \frac{(n-1)K_m + K_f + (n-1)\emptyset_f\ (K_f - K_m)}{(n-1)K_m + K_f - \emptyset_f\ (K_f - K_m)} K_m$$	A more general equation of thermal conductivity of composite which takes particle shape into account is derived by Hamilton and Crosser
Y.Agari model[193, 194]	$$\lg K_c = \phi_f C_2 \lg K_f + (1 - \phi_f)\lg(C_1 K_m)$$ For fibrous fillers: $$\lg K_c = \phi_f\left[C_2 \lg\left(\frac{L}{D}\right) + E\right]\lg K_f + (1 - \phi_f)\lg(C_1 K_m)$$	Series-parallel model is referred to by Y.Agari. The model is obtained by considering the factors of polymer crystallinity and crystal size. C_1—Factors affecting the crystallinity and crystal size of the polymer; C_2—Free factor to form conduction chain, which reflects the difficulty to form conduction chain，$0 \le C_2 \le 1$. L/D is length diameter ratio of short fiber, C is the parameter related to fiber type and E is the parameter related to dispersion type.
Hasselman-Johnson-Benvensite equation [188]	$$Kc = \frac{[2K_m + K_f(1 + 2\alpha)] + 2\emptyset_f[K_f(1 - \alpha) - K_m]}{[2K_m + K_f(1 + 2\alpha)] - 2\emptyset_f[K_f(1 - \alpha) - K_m]} K_m$$	Thermal conduction of composite is derived through Maxwell equations when spherical particles randomly distributed in a continuous matrix, particle spacing is far enough, interface thermal resistance exists between particle and matrix.
Every-Tzou-Hasselman equation[191]	$$(1 - \emptyset_f)^3 = \left(\frac{K_m}{K_c}\right)^{(1+2\alpha)/(1-\alpha)}\left(\frac{K_c - K_f(1-\alpha)}{K_m - K_f(1-\alpha)}\right)^{3/(1-\alpha)}$$ If the interface resistance does not exist, $\alpha = 0$	Based on Bruggeman method, it is usable for composites with high particle content, thermal conduction of particle and matrix interface thermal resistance
Yu model[196]	$$\frac{K_c}{K_m} = \frac{S}{(1 - \Phi)^{3(1-\alpha)/(1+2\alpha)}}$$	Yu proposed a modified Every modelto take into account the synergistic effect of graphene and Al$_2$O$_3$ particles on the composite. S is the synergistic factor, Φ is the volume fraction of the filler, α is related to thermal boundary resistance of fillers and polymer matrix
Jiajun Wang model[197]	1. $$Kc = \frac{[(n-1)K_m + K_f(1+(n-1)\alpha)] + (n-1)\emptyset_f[K_f(1-\alpha) - K_m]}{[(n-1)K_m + K_f(1+(n-1)\alpha)] - \emptyset_f[K_f(1-\alpha) - K_m]} K_m$$ 2. $$(1 - \emptyset_f)^n = \left(\frac{K_m}{K_c}\right)^{(1+n\alpha-\alpha)/(1-\alpha)}\left(\frac{K_c - K_f(1-\alpha)}{K_m - K_f(1-\alpha)}\right)^{n/(1-\alpha)}$$	1. Based on Hamilton and Crosser to consider particle size，Hasselman-Johnson-Benvensite is used to consider interface thermal resistance, Maxwell equation is improved and the new equation is obtained considering both the effect of thermal resistance and the particle shape on the thermal conductivity 2. For high filler content, the improved Bruggeman equation considering both the effect of thermal resistance and the particle shape is obtained with similar method as Bruggeman.
Porfiri model[198]		This model can be applied to composites containing coated solid particles in a matrix material and can be further expanded to include additional coating layers as it assumes that there is a three-phase

		system present.
	$$\check{k}_c = (1 - f_a) + \tilde{k}_{shell}(f_a - f_{a-t}) + \tilde{k}_{core}f_{a-t} + \frac{1}{a}\sqrt{\frac{3}{4\pi}}$$ $$\left(b_{c01}\left(f_a(\tilde{k}_{shell} - 1) + f_{a-t}(\tilde{k}_{core} - \tilde{k}_{shell}) \right) \right.$$ $$\left. + c_{c01}f_a(\tilde{k}_{core} - 1) \right)$$	
Xue model[199]	$$k_c = k_m \frac{1 - f + \left(\frac{4f}{\pi}\right)\sqrt{\frac{k_f}{k_m}}\, arctg\left(\frac{\pi}{4\sqrt{\frac{k_f}{k_m}}}\right)}{1 - f + \left(\frac{4f}{\pi}\right)\sqrt{\frac{k_m}{k_f}}\, arctg\left(\frac{\pi}{4\sqrt{\frac{k_f}{k_m}}}\right)}$$	The model of effective thermal conductivity of CNTs-based composites considers the CNTs orientation distribution. Effective for >1 vol% of CNTs in composites
Nan model[200]	$$\frac{K_c}{K_m} = 1 + \frac{fp}{3}\frac{K_f / K_m}{p + \frac{2a_K}{d}\frac{K_f}{K_m}}$$	In the model, a complete theoretical analysis of the thermal transport behaviour of CNTs is made. It predicts the degradation on the thermal behaviour arising from the interface thermal resistance exhibited between the CNTs and polymer matrix
Shahil model[201]	$$K_c = K_f\left[\frac{3K_m + 2f(K_f - K_m)}{(3 - f)K_f + K_m f + \frac{R_B K_m K_f f}{H}}\right]$$	Shahil's model improves Nan's model by treating the graphene layers as the thickness of graphene. The size, aspect ratio and thermal boundary resistance at the graphene/matrix interface are also considered in this model. Here RB is TBR at the graphene/matrix interface.
X Shen model[202]	$$k_{eff}(n)$$ $$= k_m \frac{3 + f\left[2\frac{k_Z^C(n) - k_m}{k_m + L_z(k_Z^C(n) - k_m)}(1 - L_z) + \frac{k_x^C(n) - k_m}{k_m + L_x(k_x^C(n) - k_m)}(1 - L_x)\right]}{3 - f\left(2\frac{k_Z^C(n) - k_m}{k_m + L_z(k_Z^C(n) - k_m)}L_y + \frac{k_x^C(n) - k_m}{k_m + L_x(k_x^C(n) - k_m)}L_x\right)}$$	A three dimensional model used to determine thermal conductivity of GNPs. It improved Nan's model by introducing the number of graphene layers and the lateral size to calculate the macroscopic coefficients. k_i^c is the equivalent TC of composites along the i-axis.
X Wang model[203]	$$K_c = B_0 K_m + B_1 K_m V_f + B_2 K_f$$	A general model designed to focus on artifical shapes of fillers and the resulting effect on the thermal conductivity of the composite materials. B₀, B₁ and B₂ are coefficients that vary with the shape of

		the particles according to experiment.
L Chen model[204]	$k_{eff,x} = k_{\xi-\zeta}^c cos^2\alpha + k_\eta^c sin^2\alpha$ （2a） $k_{eff,z} = k_{\xi-\zeta}^c sin^2\alpha + k_\eta^c cos^2\alpha$ （2b） where $k_\eta^c = \dfrac{H}{\dfrac{2\delta_H}{k_m} + \dfrac{2LWb}{2LWk_m + \sqrt{3}\cdot a^2(k_{p,\eta}-k_m)}}$ $k_{\xi-\zeta}^c = \dfrac{1}{2}\left[\dfrac{L}{\dfrac{2\delta_L}{k_m} + \dfrac{2LWa}{2HWk_m + \sqrt{3}\cdot ab(k_{p,\zeta-\zeta}-k_m)}} + \right.$ $\left. \dfrac{W}{\dfrac{2\delta_W}{k_m} + \dfrac{2LHa}{\sqrt{3}HLk_m + 0.75\sqrt{3}\cdot ab(k_{p,\eta}-k_m)}}\right]$	This model was for calculating the thermal conductivity of aligned hexagonal boron nitride (h-BN) platelet polymer composites by the unit cell method. Here k_η^c and $k_{\xi-\zeta}^c$ are the enhanced thermal conductivities of the unit cell along the η direction and in the $\xi-\zeta$ plane.
Chu model[205]	$\dfrac{K_c}{K_m} = \dfrac{3 + 2\eta^2 f / \left[K_m\left(2R_k/L + 13.4\sqrt{t}\right)\right]}{3 - \eta t}$	Due to the irregularity of GNPs, a surface flatness ratio is introduced to theoretically analyze the thermal conductivity of GNP composites. The model shows that higher flatness ratios (η) lead to better thermal conductivity enhancement. R_K is the filler-matrix interfacial thermal resistance, f is the filler volume fraction

Conducting particles
- Carbonaceous materials
- Metallic particles
- Conducting polymers

Polymers
- Thermoplastics
- Elastomers
- Thermosets

Functions of non-conducting particles
- Template
- Dispersant
- Reinforcement
- Additional functions
(thermal, magnetic, light, etc)

(A) Hybrid fillers

(B) Phase morphology transition

Kinetic and thermodynamic control

capacitive

Increase phase ratio

Selective dispersion of fillers

conductive

Double percolation

Segregation structure

2D nanoplatelet: clay, graphene, SiC, BN
CNT
Cellulose whisker
Carbon black, metal particles
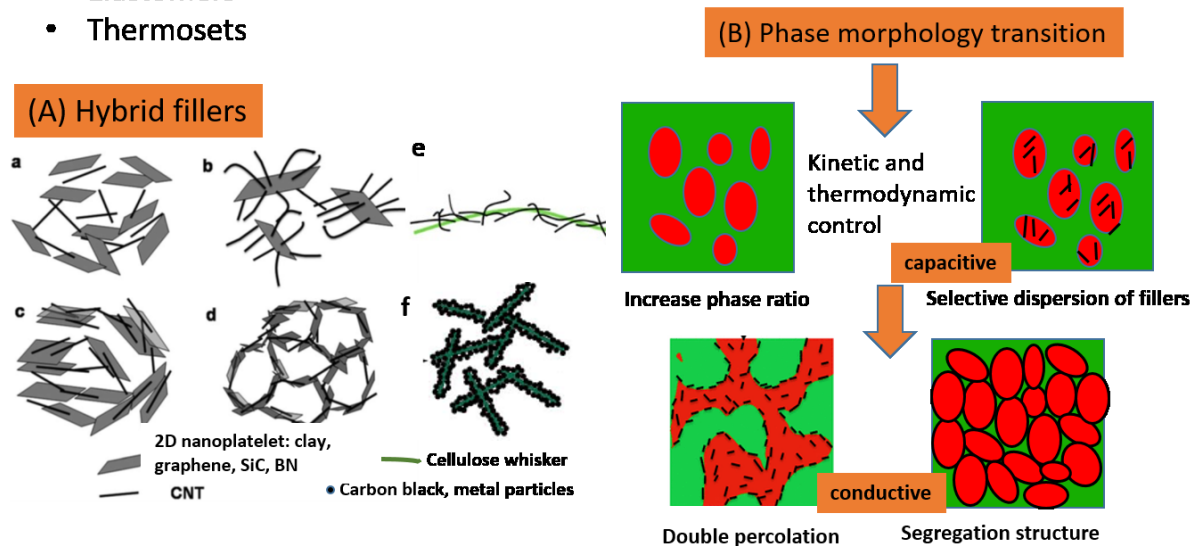
Figure 22 Schematics showing (A) assembly and dispersion morphology of hybrid fillers in polymers (adapted with permission from Tang et al[54]. Copyright 2014 Royal Society of Chemistry), and (B) phase morphology development of polymer blends in the presence of fillers.

4. Conclusions

Electrically and thermally conductive polymer composites continue to find important applications in energy, transportation, electronics, shielding and structural health monitoring for next generation infrastructure. For shielding applications, the electrical conductivity and EMI shielding performance of polymer composites are highly dependent on the selection of electrically conductive fillers, their dispersion and interfacial interactions with polymers, along with the phase morphology of the composites.

To reduce the percolation threshold (φ_c), different strategies have been investigated including

using high quality conducting fillers (CNTs or graphene), increasing the aspect ratio of the fillers, alignment of the fillers and using a combination of different types of fillers. The latest developments of these approaches have been discussed and also present in Figure 26, including;

i. the dispersion and distribution of functional fillers can be controlled by surface modification and processing conditions;

ii. selectively locating fillers in one of the phases or at the interface of polymer blends can reduce the φ_c and achieve high electrical conductivities, noting that the morphology of polymer composites are also affected by processing history, such as mixing time, shear rate and mixing sequence;

iii. the φ_c can be further reduced when fillers are selectively trapped at the interface of co-continuous polymer phases, or form an ordered network creating segregated systems, where a double- or triple- percolation threshold can often be observed[88]. Immiscible polymers with co-continuous phase morphologies are utilised in order to create a percolative polymer phase where the selective localisation of conductive fillers in one of the percolative polymer phases or at the interfaces leads to the generation of a continuous conductive path at a reduced φ_c. Kinetically this morphology requires high shear rate processing or injection moulding to complete the formation of the co-continuous phases in the composite;

iv. composites containing multiple filler types with different dimensions, aspect ratios and properties can be located within different polymer phases and generate synergistic effects on conductivity, magnetic and mechanical properties, which has found applications in EMI shielding applications (Table 6).

The thermal conductivity of polymer composites containing metallic fillers and the

chronological development of the theoretical models used to predict thermal conductivity were also discussed. Unlimited possibilities are envisioned when such hybrid composites are designed with proper configurations, such as layer-by-layer sandwich structures, fibre- or foam-like design, which are preferable for lightweight and multifunctional engineering systems.

References

1. Janoschka T, Hager MD, Schubert US. Powering up the Future: Radical Polymers for Battery Applications. Advanced Materials. 2012;24(48):6397-6409. doi: 10.1002/adma.201203119.
2. Carmona F. Conducting filled polymers. Physica A: Statistical Mechanics and its Applications. 1989;157(1):461-469.
3. Viswanathan K, Ravi T, Thirusakthimurugan P, et al. Carbon Nanotube Embedded Smart Polymer Composite for Strain and Piezo-Resistive Data Transducer Application. Materials Today: Proceedings. 2018 2018/01/01/;5(9, Part 1):17247-17252. doi: https://doi.org/10.1016/j.matpr.2018.04.135.
4. Peng C, Zhang S, Jewell D, et al. Carbon nanotube and conducting polymer composites for supercapacitors. Progress in Natural Science. 2008;18(7):777-788.
5. Dubal DP, Chodankar NR, Kim D-H, et al. Towards flexible solid-state supercapacitors for smart and wearable electronics [10.1039/C7CS00505A]. Chemical Society Reviews. 2018;47(6):2065-2129. doi: 10.1039/C7CS00505A.
6. Chen C, Tang Y, Ye YS, et al. High-performance epoxy/silica coated silver nanowire composites as underfill material for electronic packaging. Composites Science and Technology. 2014;105:80-85.
7. Yeetsorn R, Fowler M. Resistance Measurement of Conductive Thermoplastic Bipolar Plates for Polymer Electrolyte Membrane Fuel Cells. King Mongkut's University of Technology North Bangkok International Journal of Applied Science and Technology. 2014;7(4):13-21.
8. Taherian R. A review of composite and metallic bipolar plates in proton exchange membrane fuel cell: Materials, fabrication, and material selection. Journal of Power Sources. 2014 2014/11/01/;265(Supplement C):370-390. doi: https://doi.org/10.1016/j.jpowsour.2014.04.081.
9. Yeetsorn R, Fowler MW, Tzoganakis C. A Review of Thermoplastic Composites for Bipolar Plate Materials in PEM Fuel Cells. In: Cuppoletti J, editor. Nanocomposites with Unique Properties and Applications in Medicine and Industry. Rijeka: InTech; 2011. p. Ch. 16.
10. Dagdeviren C, Joe P, Tuzman OL, et al. Recent progress in flexible and stretchable piezoelectric devices for mechanical energy harvesting, sensing and actuation. Extreme Mechanics Letters. 2016 2016/12/01/;9(Part 1):269-281. doi: https://doi.org/10.1016/j.eml.2016.05.015.
11. Liu Y, Pharr M, Salvatore GA. Lab-on-Skin: A Review of Flexible and Stretchable Electronics for Wearable Health Monitoring. ACS Nano. 2017 2017/10/24;11(10):9614-9635. doi: 10.1021/acsnano.7b04898.

12.	Choi S, Lee H, Ghaffari R, et al. Recent Advances in Flexible and Stretchable Bio-Electronic Devices Integrated with Nanomaterials. Advanced Materials. 2016;28(22):4203-4218. doi: 10.1002/adma.201504150.

13.	Gubbels F, Jerome R, Vanlathem E, et al. Kinetic and Thermodynamic Control of the Selective Localization of Carbon Black at the Interface of Immiscible Polymer Blends. Chemistry of Materials. 1998 1998/05/01;10(5):1227-1235. doi: 10.1021/cm970594d.

14.	Bloor D, Donnelly K, Hands P, et al. A metal–polymer composite with unusual properties. Journal of Physics D: Applied Physics. 2005;38(16):2851.

15.	Rico Z, Christian K, Ubaid K, et al. The role of multi-walled carbon nanotubes in epoxy nanocomposites and resin transfer molded glass fiber hybrid composites: Dispersion, local distribution, thermal, and fracture/mechanical properties. Polymer Composites. 2017;38(9):1849-1863. doi: doi:10.1002/pc.23755.

16.	Yourdkhani M, Hubert P. Quantitative dispersion analysis of inclusions in polymer composites. ACS applied materials & interfaces. 2012;5(1):35-41.

17.	Ma P-C, Siddiqui NA, Marom G, et al. Dispersion and functionalization of carbon nanotubes for polymer-based nanocomposites: A review. Composites Part A: Applied Science and Manufacturing. 2010 2010/10/01/;41(10):1345-1367. doi: https://doi.org/10.1016/j.compositesa.2010.07.003.

18.	Kim SW, Kim T, Kim YS, et al. Surface modifications for the effective dispersion of carbon nanotubes in solvents and polymers. Carbon. 2012 2012/01/01/;50(1):3-33. doi: https://doi.org/10.1016/j.carbon.2011.08.011.

19.	Ross RB. Metallic materials specification handbook. Springer Science & Business Media; 2013.

20.	Kaiser AB. Electronic transport properties of conducting polymers and carbon nanotubes. Reports on Progress in Physics. 2001;64(1):1.

21.	Du X, Skachko I, Barker A, et al. Approaching ballistic transport in suspended graphene. Nature nanotechnology. 2008;3(8):491-495.

22.	Koo JH. Polymer nanocomposites. McGraw-Hill Professional Pub.; 2006.

23.	Bauhofer W, Kovacs JZ. A review and analysis of electrical percolation in carbon nanotube polymer composites. Composites Science and Technology. 2009 2009/08/01/;69(10):1486-1498. doi: https://doi.org/10.1016/j.compscitech.2008.06.018.

24.	Singh BP, Saini K, Choudhary V, et al. Effect of length of carbon nanotubes on electromagnetic interference shielding and mechanical properties of their reinforced epoxy composites [journal article]. Journal of Nanoparticle Research. 2013 December 07;16(1):2161. doi: 10.1007/s11051-013-2161-9.

25.	Khan SU, Pothnis JR, Kim J-K. Effects of carbon nanotube alignment on electrical and mechanical properties of epoxy nanocomposites. Composites Part A: Applied Science and Manufacturing. 2013 2013/06/01/;49(Supplement C):26-34. doi: https://doi.org/10.1016/j.compositesa.2013.01.015.

26.	Al-Saleh MH, Sundararaj U. A review of vapor grown carbon nanofiber/polymer conductive composites. Carbon. 2009;47(1):2-22.

27.	Janssen H-K, Täuber UC. The field theory approach to percolation processes. Annals of Physics. 2005;315(1):147-192.

28.	Kirkpatrick S. Percolation and Conduction. Reviews of Modern Physics. 1973 10/01/;45(4):574-588.

29.	Balberg I, Binenbaum N. Computer study of the percolation threshold in a two-dimensional anisotropic system of conducting sticks. Physical Review B. 1983 10/01/;28(7):3799-3812.

30. Marsden AJ, Papageorgiou DG, Vallés C, et al. Electrical percolation in graphene–polymer composites. 2D Materials. 2018;5(3):032003.

31. Zhang H-B, Zheng W-G, Yan Q, et al. Electrically conductive polyethylene terephthalate/graphene nanocomposites prepared by melt compounding. Polymer. 2010 2010/03/02/;51(5):1191-1196. doi: https://doi.org/10.1016/j.polymer.2010.01.027.

32. Münstedt H, Starý Z. Is electrical percolation in carbon-filled polymers reflected by rheological properties? Polymer. 2016 2016/08/19/;98(Supplement C):51-60. doi: https://doi.org/10.1016/j.polymer.2016.05.042.

33. Hoseini AHA, Arjmand M, Sundararaj U, et al. Significance of interfacial interaction and agglomerates on electrical properties of polymer-carbon nanotube nanocomposites. Materials & Design. 2017 2017/07/05/;125(Supplement C):126-134. doi: https://doi.org/10.1016/j.matdes.2017.04.004.

34. Connor MT, Roy S, Ezquerra TA, et al. Broadband ac conductivity of conductor-polymer composites. Physical Review B. 1998 01/15/;57(4):2286-2294.

35. Maiti S, Shrivastava NK, Suin S, et al. Polystyrene/MWCNT/Graphite Nanoplate Nanocomposites: Efficient Electromagnetic Interference Shielding Material through Graphite Nanoplate–MWCNT–Graphite Nanoplate Networking. ACS Applied Materials & Interfaces. 2013 2013/06/12;5(11):4712-4724. doi: 10.1021/am400658h.

36. Du F, Scogna RC, Zhou W, et al. Nanotube Networks in Polymer Nanocomposites: Rheology and Electrical Conductivity. Macromolecules. 2004 2004/11/01;37(24):9048-9055. doi: 10.1021/ma049164g.

37. Kim NH, Kuila T, Kim KM, et al. Material selection windows for hybrid carbons/poly (phenylene sulfide) composite for bipolar plates of fuel cell. Polymer Testing. 2012;31(4):537-545.

38. Cinelli M, Coles SR, Nadagouda MN, et al. A green chemistry-based classification model for the synthesis of silver nanoparticles. Green Chemistry. 2015;17(5):2825-2839.

39. Lee JH, Jang YK, Hong CE, et al. Effect of carbon fillers on properties of polymer composite bipolar plates of fuel cells. Journal of Power Sources. 2009;193(2):523-529.

40. Xiong Z-Y, Zhang B-Y, Wang L, et al. Modeling the electrical percolation of mixed carbon fillers in polymer blends. Carbon. 2014;70:233-240.

41. Pal G, Kumar S. Multiscale modeling of effective electrical conductivity of short carbon fiber-carbon nanotube-polymer matrix hybrid composites. Materials & Design. 2016 2016/01/05/;89(Supplement C):129-136. doi: https://doi.org/10.1016/j.matdes.2015.09.105.

42. Zakaria MY, Sulong AB, Sahari J, et al. Effect of the addition of milled carbon fiber as a secondary filler on the electrical conductivity of graphite/epoxy composites for electrical conductive material. Composites Part B Engineering. 2015;83:75-80.

43. Radzuan NAM, Zakaria MY, Sulong AB, et al. The effect of milled carbon fibre filler on electrical conductivity in highly conductive polymer composites. Composites Part B Engineering. 2017;110:153-160.

44. Motaghi A, Hrymak A, Motlagh GH. Electrical conductivity and percolation threshold of hybrid carbon/polymer composites. Journal of Applied Polymer Science. 2015;132(13).

45. Xu Z, Wang N, Li N, et al. Liquid sensing behaviors of conductive polypropylene composites containing hybrid fillers of carbon fiber and carbon black. Composites Part B Engineering. 2016;94:45-51.

46.   Socher R, Krause B, Hermasch S, et al. Electrical and thermal properties of polyamide 12 composites with hybrid fillers systems of multiwalled carbon nanotubes and carbon black. Composites Science and Technology. 2011;71(8):1053-1059.

47.   Zeng Z, Jin H, Chen M, et al. Lightweight and anisotropic porous MWCNT/WPU composites for ultrahigh performance electromagnetic interference shielding. Advanced Functional Materials. 2016;26(2):303-310.

48.   Lee SH, Kim JY, Koo CM, et al. Effects of processing methods on the electrical conductivity, electromagnetic parameters, and EMI shielding effectiveness of polypropylene/nickel-coated carbon fiber composites [journal article]. Macromolecular Research. 2017 September 01;25(9):936-943. doi: 10.1007/s13233-017-5113-x.

49.   Wang P, Zhang J, Dong L, et al. Interlayer Polymerization in Chemically Expanded Graphite for Preparation of Highly Conductive, Mechanically Strong Polymer Composites. Chemistry of Materials. 2017 2017/04/25;29(8):3412-3422. doi: 10.1021/acs.chemmater.6b04734.

50.   Wang B, Li J, Liu Y, et al. Reduced graphene oxide/carbon nanotubes nanohybrids as preformed reinforcement for polystyrene composites. Journal of Applied Polymer Science. 2017;134(28).

51.   Ling J, Zhai W, Feng W, et al. Facile Preparation of Lightweight Microcellular Polyetherimide/Graphene Composite Foams for Electromagnetic Interference Shielding. ACS Applied Materials & Interfaces. 2013 2013/04/10;5(7):2677-2684. doi: 10.1021/am303289m.

52.   Zhao B, Zhao C, Li R, et al. Flexible, Ultrathin, and High-Efficiency Electromagnetic Shielding Properties of Poly(Vinylidene Fluoride)/Carbon Composite Films. ACS Applied Materials & Interfaces. 2017 2017/06/21;9(24):20873-20884. doi: 10.1021/acsami.7b04935.

53.   Hua J, Li Y, Liu X, et al. Graphene/MWNT/Poly(p-phenylenebenzobisoxazole) Multiphase Nanocomposite via Solution Prepolymerization with Superior Microwave Absorption Properties and Thermal Stability. The Journal of Physical Chemistry C. 2017 2017/01/19;121(2):1072-1081. doi: 10.1021/acs.jpcc.6b11925.

54.   Tang C, Long G, Hu X, et al. Conductive polymer nanocomposites with hierarchical multi-scale structures via self-assembly of carbon-nanotubes on graphene on polymer-microspheres [10.1039/C3NR06056J]. Nanoscale. 2014;6(14):7877-7888. doi: 10.1039/C3NR06056J.

55.   Li X-H, He Y, Li X, et al. Simultaneous Enhancements in Toughness and Electrical Conductivity of Polypropylene/Carbon Nanotube Nanocomposites by Incorporation of Electrically Inert Calcium Carbonate Nanoparticles. Industrial & Engineering Chemistry Research. 2017 2017/03/15;56(10):2783-2788. doi: 10.1021/acs.iecr.7b00446.

56.   Wu X, Lu C, Zhang X, et al. Conductive natural rubber/carbon black nanocomposites via cellulose nanowhisker templated assembly: tailored hierarchical structure leading to synergistic property enhancements [10.1039/C5TA02601F]. Journal of Materials Chemistry A. 2015;3(25):13317-13323. doi: 10.1039/C5TA02601F.

57.   Xu S, Yu W, Jing M, et al. Largely Enhanced Stretching Sensitivity of Polyurethane/Carbon Nanotube Nanocomposites via Incorporation of Cellulose Nanofiber. The Journal of Physical Chemistry C. 2017 2017/02/02;121(4):2108-2117. doi: 10.1021/acs.jpcc.6b11783.

58.   Oxfall H, Ariu G, Gkourmpis T, et al. Effect of carbon black on electrical and rheological properties of graphite nanoplatelets/poly (ethylene-butyl acrylate) composites. Express Polymer Letters. 2015;9(1):66-76.

59.   Akın D, Kasgoz A, Durmus A. Quantifying microstructure, electrical and mechanical properties of carbon fiber and expanded graphite filled cyclic olefin copolymer composites. Composites Part A Applied Science & Manufacturing. 2014;60(3):44-51.

60.   Kakati BK, Ghosh A, Verma A. Efficient composite bipolar plate reinforced with carbon fiber and graphene for proton exchange membrane fuel cell. International Journal of Hydrogen Energy. 2013;38(22):9362-9369.

61.   E. Bekyarova, E. T. Thostenson, A. Yu, et al. Multiscale Carbon Nanotube−Carbon Fiber Reinforcement for Advanced Epoxy Composites. Langmuir the Acs Journal of Surfaces & Colloids. 2007;23(7):3970-4.

62.   Li J, Favis B. Characterizing co-continuous high density polyethylene/polystyrene blends. Polymer. 2001;42(11):5047-5053.

63.   Xiu H, Zhou Y, Dai J, et al. Formation of new electric double percolation via carbon black induced co-continuous like morphology [10.1039/C4RA06836J]. RSC Advances. 2014;4(70):37193-37196. doi: 10.1039/C4RA06836J.

64.   Cardinaud R, McNally T. Localization of MWCNTs in PET/LDPE blends. European Polymer Journal. 2013 2013/06/01/;49(6):1287-1297. doi: https://doi.org/10.1016/j.eurpolymj.2013.01.007.

65.   Mekhilef N, Verhoogt H. Phase inversion and dual-phase continuity in polymer blends: theoretical predictions and experimental results. Polymer. 1996;37(18):4069-4077.

66.   Wiwattananukul R, Hachiya Y, Nobukawa S, et al. Selective localization of carbon nanotubes in PC/PET blends. Polymer Composites. 2015.

67.   Otero-Navas I, Arjmand M, Sundararaj U. Carbon nanotube induced double percolation in polymer blends: Morphology, rheology and broadband dielectric properties. Polymer. 2017 2017/04/07/;114(Supplement C):122-134. doi: https://doi.org/10.1016/j.polymer.2017.02.082.

68.   Wu S. Calculation of interfacial tension in polymer systems. Journal of Polymer Science Part C: Polymer Symposia. 1971;34(1):19-30. doi: 10.1002/polc.5070340105.

69.   Sumita M, Sakata K, Asai S, et al. Dispersion of fillers and the electrical conductivity of polymer blends filled with carbon black [journal article]. Polymer Bulletin. 1991 February 01;25(2):265-271. doi: 10.1007/bf00310802.

70.   Wu S. Interfacial and Surface Tensions of Polymers. Journal of Macromolecular Science, Part C. 1974 1974/01/01;10(1):1-73. doi: 10.1080/15321797408080004.

71.   Zhang Q, Wang J, Yu J, et al. Improved electrical conductivity of TPU/carbon black composites by addition of COPA and selective localization of carbon black at the interface of sea-island structured polymer blends [10.1039/C7SM00346C]. Soft Matter. 2017;13(18):3431-3439. doi: 10.1039/C7SM00346C.

72.   Bai L, Sharma R, Cheng X, et al. Kinetic Control of Graphene Localization in Co-continuous Polymer Blends via Melt Compounding. Langmuir. 2017 2017/10/16. doi: 10.1021/acs.langmuir.7b03085.

73.   Huang J, Mao C, Zhu Y, et al. Control of carbon nanotubes at the interface of a co-continuous immiscible polymer blend to fabricate conductive composites with ultralow percolation thresholds. Carbon. 2014 2014/07/01/;73(Supplement C):267-274. doi: https://doi.org/10.1016/j.carbon.2014.02.063.

74.   Al-Saleh MH, Sundararaj U. An innovative method to reduce percolation threshold of carbon black filled immiscible polymer blends. Composites Part A: Applied Science and Manufacturing. 2008 2008/02/01/;39(2):284-293. doi: https://doi.org/10.1016/j.compositesa.2007.10.010.

75. Chen J, Cui X, Zhu Y, et al. Design of superior conductive polymer composite with precisely controlling carbon nanotubes at the interface of a co-continuous polymer blend via a balance of π-π interactions and dipole-dipole interactions. Carbon. 2017 2017/04/01;114(Supplement C):441-448. doi: https://doi.org/10.1016/j.carbon.2016.12.048.

76. Tan Y, Fang L, Xiao J, et al. Grafting of copolymers onto graphene by miniemulsion polymerization for conductive polymer composites: improved electrical conductivity and compatibility induced by interfacial distribution of graphene [10.1039/C3PY00164D]. Polymer Chemistry. 2013;4(10):2939-2944. doi: 10.1039/C3PY00164D.

77. Mao C, Zhu Y, Jiang W. Design of Electrical Conductive Composites: Tuning the Morphology to Improve the Electrical Properties of Graphene Filled Immiscible Polymer Blends. ACS Applied Materials & Interfaces. 2012 2012/10/24;4(10):5281-5286. doi: 10.1021/am301230q.

78. Gegenhuber T, Krekhova M, Schöbel J, et al. "Patchy" Carbon Nanotubes as Efficient Compatibilizers for Polymer Blends. ACS Macro Letters. 2016 2016/03/15;5(3):306-310. doi: 10.1021/acsmacrolett.6b00033.

79. Zhang T, Yang J, Zhang N, et al. Achieving Large Dielectric Property Improvement in Poly(ethylene vinyl acetate)/Thermoplastic Polyurethane/Multiwall Carbon Nanotube Nanocomposites by Tailoring Phase Morphology. Industrial & Engineering Chemistry Research. 2017 2017/04/05;56(13):3607-3617. doi: 10.1021/acs.iecr.6b04763.

80. Scherzer SL, Pavlova E, Esper JD, et al. Phase structure, rheology and electrical conductivity of co-continuous polystyrene/polymethylmethacrylate blends filled with carbon black. Composites Science and Technology. 2015 2015/11/23/;119(Supplement C):138-147. doi: https://doi.org/10.1016/j.compscitech.2015.10.003.

81. Bose S, Sharma M, Bharati A, et al. A strategy to achieve enhanced electromagnetic interference shielding at ultra-low concentration of multiwall carbon nanotubes in P[small alpha]MSAN/PMMA blends in the presence of a random copolymer PS-r-PMMA [10.1039/C5RA27976C]. RSC Advances. 2016;6(32):26959-26966. doi: 10.1039/C5RA27976C.

82. Bai L, He S, Fruehwirth JW, et al. Localizing graphene at the interface of cocontinuous polymer blends: Morphology, rheology, and conductivity of cocontinuous conductive polymer composites. Journal of Rheology. 2017;61(4):575-587.

83. Shi Y-D, Lei M, Chen Y-F, et al. Ultralow Percolation Threshold in Poly(l-lactide)/Poly(ε-caprolactone)/Multiwall Carbon Nanotubes Composites with a Segregated Electrically Conductive Network. The Journal of Physical Chemistry C. 2017 2017/02/09;121(5):3087-3098. doi: 10.1021/acs.jpcc.6b11351.

84. Wu M, Shaw LL. A novel concept of carbon-filled polymer blends for applications in PEM fuel cell bipolar plates. International Journal of Hydrogen Energy. 2005;30(4):373-380.

85. Phuttachart T, Kreua-ongarjnukool N, Yeetsorn R, et al. PMMA/PU/CB composite bipolar plate for direct methanol fuel cell. Energy procedia. 2014;52:516-524.

86. Yuan J-K, Yao S-H, Sylvestre A, et al. Biphasic polymer blends containing carbon nanotubes: heterogeneous nanotube distribution and its influence on the dielectric properties. The Journal of Physical Chemistry C. 2012;116(2):2051-2058.

87.   Thongruang W, Spontak RJ, Balik CM. Bridged double percolation in conductive polymer composites: an electrical conductivity, morphology and mechanical property study. Polymer. 2002;43(13):3717-3725.

88.   Sumita M, Sakata K, Hayakawa Y, et al. Double percolation effect on the electrical conductivity of conductive particles filled polymer blends. Colloid and Polymer Science. 1992;270(2):134-139.

89.   Al-Saleh MH, Al-Anid HK, Hussain YA. Electrical double percolation and carbon nanotubes distribution in solution processed immiscible polymer blend. Synthetic Metals. 2013;175:75-80.

90.   Cui L, Zhang Y, Zhang Y, et al. Electrical properties and conductive mechanisms of immiscible polypropylene/Novolac blends filled with carbon black. European Polymer Journal. 2007;43(12):5097-5106.

91.   Pisitsak P, Magaraphan R, Jana SC. Electrically conductive compounds of polycarbonate, liquid crystalline polymer, and multiwalled carbon nanotubes. Journal of Nanomaterials. 2012;2012:2.

92.   Dai K, Xu X-B, Li Z-M. Electrically conductive carbon black (CB) filled in situ microfibrillar poly (ethylene terephthalate)(PET)/polyethylene (PE) composite with a selective CB distribution. Polymer. 2007;48(3):849-859.

93.   Naficy S, Garmabi H. Study of the effective parameters on mechanical and electrical properties of carbon black filled PP/PA6 microfibrillar composites. Composites science and technology. 2007;67(15):3233-3241.

94.   Kim JH, Son K, Lee M. Properties of Nanocomposites Based on Polymer Blend Containing PVDF, Carbon Fiber and Carbon Nanotube. Journal of the Korean Industrial & Engineering Chemistry. 2014;25(1):14-19.

95.   Gao X, Zhang S, Mai F, et al. Preparation of high performance conductive polymer fibres from double percolated structure. Journal of Materials Chemistry. 2011;21(17):6401-6408.

96.   Zhang C, Yi X-S, Yui H, et al. Selective location and double percolation of short carbon fiber filled polymer blends: high-density polyethylene/isotactic polypropylene. Materials Letters. 1998;36(1):186-190.

97.   Pang H, Yan D-X, Bao Y, et al. Super-tough conducting carbon nanotube/ultrahigh-molecular-weight polyethylene composites with segregated and double-percolated structure. Journal of Materials Chemistry. 2012;22(44):23568-23575.

98.   Scherzer SL, Pavlova E, Esper JD, et al. Phase structure, rheology and electrical conductivity of co-continuous polystyrene/polymethylmethacrylate blends filled with carbon black. Composites Science and Technology. 2015;119:138-147.

99.   Poyekar AV, Bhattacharyya AR, Khare RA, et al. Dispersion, migration, and 'network-like' structure formation of multiwall carbon nanotubes in co-continuous, binary immiscible blends of polyamide 6 and acrylonitrile–butadiene–styrene copolymer during simultaneous melt-mixing. Polymer Engineering & Science. 2015;55(2):443-456.

100.   Ma Y, Wu D, Liu Y, et al. Electrically conductive and super-tough polypropylene/carbon nanotube nanocomposites prepared by melt compounding. Composites Part B. 2014;56(1):384-391.

101.   Shi YD, Lei M, Chen YF, et al. Ultralow Percolation Threshold in Poly(L-lactide)/Poly(ε-caprolactone)/Multi-Wall Carbon Nanotubes Composites with a Segregated Electrically Conductive Network. Journal of Physical Chemistry C. 2017.

102.   Hsieh CT, Pan YJ, Lin JH. Polypropylene/high-density polyethylene/carbon fiber composites: Manufacturing techniques, mechanical properties, and electromagnetic interference shielding effectiveness. Fibers & Polymers. 2017;18(1):155-161.

103. Egurrola SL, Castro TDC, Ortega MMC, et al. Electrical, mechanical, and piezoresistive properties of carbon nanotube–polyaniline hybrid filled polydimethylsiloxane composites. Journal of Applied Polymer Science. 2017;134(18):44780-44789.

104. Mamunya Y, Levchenko V, Boiteux G, et al. Controlling morphology, electrical, and mechanical properties of polymer blends by heterogeneous distribution of carbon nanotubes. Polymer Composites. 2016;37(8):2467-2477.

105. Roman C, García-Morales M, Gupta J, et al. On the phase affinity of multi-walled carbon nanotubes in PMMA:LDPE immiscible polymer blends. Polymer. 2017 2017/06/02/;118(Supplement C):1-11. doi: https://doi.org/10.1016/j.polymer.2017.04.050.

106. Pang H, Xu L, Yan D-X, et al. Conductive polymer composites with segregated structures. Progress in Polymer Science. 2014;39(11):1908-1933.

107. Li T, Ma L-F, Bao R-Y, et al. A new approach to construct segregated structures in thermoplastic polyolefin elastomers towards improved conductive and mechanical properties [10.1039/C5TA00314H]. Journal of Materials Chemistry A. 2015;3(10):5482-5490. doi: 10.1039/C5TA00314H.

108. Jia L-C, Yan D-X, Cui C-H, et al. Electrically conductive and electromagnetic interference shielding of polyethylene composites with devisable carbon nanotube networks [10.1039/C5TC01822F]. Journal of Materials Chemistry C. 2015;3(36):9369-9378. doi: 10.1039/C5TC01822F.

109. Wang Y, Gu F-q, Ni L-j, et al. Easily fabricated and lightweight PPy/PDA/AgNW composites for excellent electromagnetic interference shielding [10.1039/C7NR05951E]. Nanoscale. 2017. doi: 10.1039/C7NR05951E.

110. Hsiao S-T, Ma C-CM, Tien H-W, et al. Effect of Covalent Modification of Graphene Nanosheets on the Electrical Property and Electromagnetic Interference Shielding Performance of a Water-Borne Polyurethane Composite. ACS Applied Materials & Interfaces. 2015 2015/02/04;7(4):2817-2826. doi: 10.1021/am508069v.

111. Gupta TK, Singh BP, Singh VN, et al. MnO2 decorated graphene nanoribbons with superior permittivity and excellent microwave shielding properties [10.1039/C3TA14854H]. Journal of Materials Chemistry A. 2014;2(12):4256-4263. doi: 10.1039/C3TA14854H.

112. Bhattacharjee Y, Arief I, Bose S. Recent trends in multi-layered architectures towards screening electromagnetic radiation: challenges and perspectives [10.1039/C7TC02172K]. Journal of Materials Chemistry C. 2017;5(30):7390-7403. doi: 10.1039/C7TC02172K.

113. Bhattacharya S, Chaklader A. Review on metal-filled plastics. Part1. Electrical conductivity. Polymer-Plastics Technology and Engineering. 1982;19(1):21-51.

114. Park S-J, Kim H-C, Kim H-Y. Roles of work of adhesion between carbon blacks and thermoplastic polymers on electrical properties of composites. Journal of colloid and interface science. 2002;255(1):145-149.

115. Bigg Battelle DM. Conductive polymeric compositions. Polymer Engineering & Science. 1977;17(12):842-847.

116. Luyt A, Molefi J, Krump H. Thermal, mechanical and electrical properties of copper powder filled low-density and linear low-density polyethylene composites. Polymer Degradation and Stability. 2006;91(7):1629-1636.

117. Alvarez M, Poblete V, Pilleux M, et al. Submicron copper-low-density polyethylene conducting composites: Structural, electrical, and percolation threshold. Journal of applied polymer science. 2006;99(6):3005-3008.

118. Huang W, Li J, Zhao S, et al. Highly electrically conductive and stretchable copper nanowires-based composite for flexible and printable electronics. Composites Science & Technology. 2017.

119. Krupa I, Cecen V, Boudenne A, et al. The mechanical and adhesive properties of electrically and thermally conductive polymeric composites based on high density polyethylene filled with nickel powder. Materials & Design. 2013;51:620-628.

120. Xu H-P, Dang Z-M, Bing N-C, et al. Temperature dependence of electric and dielectric behaviors of Ni/polyvinylidene fluoride composites. Journal of Applied Physics. 2010;107(3):034105.

121. Panda M, Srinivas V, Thakur A. Surface and interfacial effect of filler particle on electrical properties of polyvinyledene fluoride/nickel composites. Applied Physics Letters. 2008;93(24):242908.

122. Biswas S, Arief I, Panja SS, et al. Absorption-Dominated Electromagnetic Wave Suppressor Derived from Ferrite-Doped Cross-Linked Graphene Framework and Conducting Carbon. ACS Applied Materials & Interfaces. 2017 2017/01/25;9(3):3030-3039. doi: 10.1021/acsami.6b14853.

123. Biswas S, Panja SS, Bose S. Unique Multilayered Assembly Consisting of "Flower-Like" Ferrite Nanoclusters Conjugated with MWCNT as Millimeter Wave Absorbers. The Journal of Physical Chemistry C. 2017 2017/07/06;121(26):13998-14009. doi: 10.1021/acs.jpcc.7b02668.

124. Biswas S, Kar GP, Bose S. Tailor-Made Distribution of Nanoparticles in Blend Structure toward Outstanding Electromagnetic Interference Shielding. ACS Applied Materials & Interfaces. 2015 2015/11/18;7(45):25448-25463. doi: 10.1021/acsami.5b08333.

125. Lakshmi NV, Tambe P. EMI shielding effectiveness of graphene decorated with graphene quantum dots and silver nanoparticles reinforced PVDF nanocomposites. Composite Interfaces. 2017 2017/11/22;24(9):861-882. doi: 10.1080/09276440.2017.1302202.

126. Wang G-S, Wu Y, Wei Y-Z, et al. Fabrication of Reduced Graphene Oxide (RGO)/Co3O4 Nanohybrid Particles and a RGO/Co3O4/Poly(vinylidene fluoride) Composite with Enhanced Wave-Absorption Properties. ChemPlusChem. 2014;79(3):375-381. doi: 10.1002/cplu.201300345.

127. Zhang X-J, Wang G-S, Cao W-Q, et al. Enhanced Microwave Absorption Property of Reduced Graphene Oxide (RGO)-MnFe2O4 Nanocomposites and Polyvinylidene Fluoride. ACS Applied Materials & Interfaces. 2014 2014/05/28;6(10):7471-7478. doi: 10.1021/am500862g.

128. Srivastava RK, Xavier P, Gupta SN, et al. Excellent Electromagnetic Interference Shielding by Graphene- MnFe2O4-Multiwalled Carbon Nanotube Hybrids at Very Low Weight Percentage in Polymer Matrix. ChemistrySelect. 2016;1(18):5995-6003. doi: 10.1002/slct.201601302.

129. Arief I, Biswas S, Bose S. FeCo-Anchored Reduced Graphene Oxide Framework-Based Soft Composites Containing Carbon Nanotubes as Highly Efficient Microwave Absorbers with Excellent Heat Dissipation Ability. ACS Applied Materials & Interfaces. 2017 2017/06/07;9(22):19202-19214. doi: 10.1021/acsami.7b04053.

130. Guo A-P, Zhang X-J, Wang S-W, et al. Excellent Microwave Absorption and Electromagnetic Interference Shielding Based on Reduced Graphene Oxide@MoS2/Poly(Vinylidene Fluoride) Composites. ChemPlusChem. 2016;81(12):1305-1311. doi: 10.1002/cplu.201600370.

131. Sun R, Zhang H-B, Liu J, et al. Highly Conductive Transition Metal Carbide/Carbonitride(MXene)@polystyrene Nanocomposites Fabricated by

Electrostatic Assembly for Highly Efficient Electromagnetic Interference Shielding. Advanced Functional Materials.1702807-n/a. doi: 10.1002/adfm.201702807.

132. Pawar SP, Bose S. Extraordinary Synergy in Attenuating Microwave Radiation with Cobalt-Decorated Graphene Oxide and Carbon Nanotubes in Polycarbonate/Poly(styrene-co-acrylonitrile) Blends. ChemNanoMat. 2015;1(8):603-614. doi: 10.1002/cnma.201500154.

133. Voet A, Whitten WN, Cook FR. Electron tunneling in carbon blacks. Colloid & Polymer Science. 1965;201(1):39-46.

134. Ezquerra TA, Kulescza M, Cruz CS, et al. Charge transport in polyethylene–graphite composite materials. Advanced Materials. 1990;2(12):597-600.

135. Scarisbrick R. Electrically conducting mixtures. Journal of Physics D: Applied Physics. 1973;6(17):2098.

136. McCullough RL. Generalized combining rules for predicting transport properties of composite materials. Composites Science and Technology. 1985;22(1):3-21.

137. Bueche F. Electrical resistivity of conducting particles in an insulating matrix. Journal of Applied Physics. 1972;43(11):4837-4838.

138. Sohi NJS, Bhadra S, Khastgir D. The effect of different carbon fillers on the electrical conductivity of ethylene vinyl acetate copolymer-based composites and the applicability of different conductivity models. Carbon. 2011;49(4):1349-1361.

139. Nurul Hidayah I, Mariatti M. Properties of single and hybrid aluminum and silver fillers filled high-density polyethylene composites. Journal of Thermoplastic Composite Materials. 2012;25(2):209-221.

140. Novák I, Žigo O, Valentin M, et al. Electrical, thermal and surface properties of nickel-based composites.

141. Rybak A, Boiteux G, Melis F, et al. Conductive polymer composites based on metallic nanofiller as smart materials for current limiting devices. Composites Science and Technology. 2010;70(2):410-416.

142. Nurazreena, Hussain LB, Ismail H, et al. Metal Filled High Density Polyethylene Composites–Electrical and Tensile Properties. Journal of Thermoplastic Composite Materials. 2006;19(4):413-425.

143. Rusu M, Sofian N, Rusu D, et al. Properties of iron powder filled high density polyethylene. Journal of polymer engineering. 2001;21(5):469-487.

144. Boiteux G, Mamunya YP, Lebedev E, et al. From conductive polymer composites with controlled morphology to smart materials. Synthetic metals. 2007;157(24):1071-1073.

145. Jouni M, Boudenne A, Boiteux G, et al. Electrical and thermal properties of polyethylene/silver nanoparticle composites. Polymer Composites. 2013;34(5):778-786.

146. Mamunya YP, Davydenko V, Pissis P, et al. Electrical and thermal conductivity of polymers filled with metal powders. European polymer journal. 2002;38(9):1887-1897.

147. Subiela J, López J, Balart R, et al. Electrical properties of EVA filled by zinc powder. Journal of materials science. 2006;41(19):6396-6402.

148. Pavlović M, Pavlović M, Ćosović V, et al. Influence of electrolytic copper powder particle morphology on electrical conductivity of lignocellulose composites and formation of conductive pathways. Int J Electrochem Sci. 2014;9:8355-8366.

149. Huang X, Jiang P, Xie L. Ferroelectric polymer/silver nanocomposites with high dielectric constant and high thermal conductivity. Applied Physics Letters. 2009;95(24):242901.

150. Al-Saleh MH, Gelves GA, Sundararaj U. Copper nanowire/polystyrene nanocomposites: lower percolation threshold and higher EMI shielding. Composites Part A: Applied Science and Manufacturing. 2011;42(1):92-97.

151. Lin B, Gelves GA, Haber JA, et al. Electrical, rheological, and mechanical properties of polystyrene/copper nanowire nanocomposites. Industrial & engineering chemistry research. 2007;46(8):2481-2487.

152. Goyal R, Kambale K, Nene S, et al. Fabrication, thermal and electrical properties of polyphenylene sulphide/copper composites. Materials Chemistry and Physics. 2011;128(1):114-120.

153. Cortes LQ, Lonjon A, Dantras E, et al. High-performance thermoplastic composites poly (ether ketone ketone)/silver nanowires: Morphological, mechanical and electrical properties. Journal of Non-Crystalline Solids. 2014;391:106-111.

154. Mamunya Y, Muzychenko Y, Lebedev E, et al. PTC effect and structure of polymer composites based on polyethylene/polyoxymethylene blend filled with dispersed iron. Polymer Engineering & Science. 2007;47(1):34-42.

155. Roussel F, King RCY, Kuriakose M, et al. Electrical and thermal transport properties of polyaniline/silver composites and their use as thermoelectric materials. Synthetic Metals. 2015;199:196-204.

156. Bhingardive V, Kulthe M. Effect of copper on the properties of copper-filled PVC composite. 2014.

157. Singh D, Singh N, Kulriya P, et al. AC electrical and structural properties of polymethylmethacrylate/aluminum composites. Journal of composite materials. 2010;44(26):3165-3178.

158. Xu H-P, Dang Z-M. Electrical property and microstructure analysis of poly (vinylidene fluoride)-based composites with different conducting fillers. Chemical physics letters. 2007;438(4):196-202.

159. Dorairajan M, Srinivas V, Raju V, et al. Temperature Dependent Electrical Properties of Green Synthesized Silver Nanoparticles-Polyaniline Composite. Advanced Materials Research. 2014;938:162–165.

160. Alsharaeh EH. Polystyrene-poly (methyl methacrylate) silver nanocomposites: Significant modification of the thermal and electrical properties by microwave irradiation. Materials. 2016;9(6):458.

161. Kim WJ, Taya M, Nguyen MN. Electrical and thermal conductivities of a silver flake/thermosetting polymer matrix composite. Mechanics of Materials. 2009;41(10):1116-1124.

162. Jouni M, Boudenne A, Boiteux G, et al. Significant enhancement of electrical and thermal conductivities of polyethylene carbon nanotube composites by the addition of a low amount of silver nanoparticles. Polymers for Advanced Technologies. 2015;25(9):1054-1059.

163. Carlberg B, Ye LL, Liu J. Polymer-metal nanofibrous composite for thermal management of microsystems. Materials Letters. 2012;75(1):229-232.

164. Krupa I, Boudenne A, Ibos L. Thermophysical properties of polyethylene filled with metal coated polyamide particles. European Polymer Journal. 2007;43(6):2443-2452.

165. Yu S, Lee JW, Han TH, et al. Copper shell networks in polymer composites for efficient thermal conduction. Applied Materials & Interfaces. 2013;5(22):11618.

166. Zhou Y, Wang H, Feng X, et al. A poly(vinylidene fluoride) composite with added self-passivated microaluminum and nanoaluminum particles for enhanced thermal conductivity. Applied Physics Letters. 2011;98(18):895.

167. Pak SY, Kim HM, Kim SY, et al. Synergistic improvement of thermal conductivity of thermoplastic composites with mixed boron nitride and multi-walled carbon nanotube

fillers. Carbon. 2012 2012/11/01/;50(13):4830-4838. doi: https://doi.org/10.1016/j.carbon.2012.06.009.

168. Leung SN, Khan MO, Chan E, et al. Synergistic effects of hybrid fillers on the development of thermally conductive polyphenylene sulfide composites. J Appl Polym Sci. 2012 2013/03/05;127(5):3293-3301. doi: 10.1002/app.37941.

169. Yoo Y, Lee HL, Ha SM, et al. Effect of graphite and carbon fiber contents on the morphology and properties of thermally conductive composites based on polyamide 6. Polym Int. 2013 2014/01/01;63(1):151-157. doi: 10.1002/pi.4534.

170. Choi SW, Yoon KH, Jeong S-S. Morphology and thermal conductivity of polyacrylate composites containing aluminum/multi-walled carbon nanotubes. Composites Part A: Applied Science and Manufacturing. 2013 2013/02/01/;45:1-5. doi: https://doi.org/10.1016/j.compositesa.2012.09.008.

171. Choi S, Kim J. Thermal conductivity of epoxy composites with a binary-particle system of aluminum oxide and aluminum nitride fillers. Composites, Part B. 2013 2013/08/01/;51:140-147. doi: https://doi.org/10.1016/j.compositesb.2013.03.002.

172. Li T-L, Hsu SL-C. Enhanced Thermal Conductivity of Polyimide Films via a Hybrid of Micro- and Nano-Sized Boron Nitride. The Journal of Physical Chemistry B. 2010 2010/05/27;114(20):6825-6829. doi: 10.1021/jp101857w.

173. Teng C-C, Ma C-CM, Chiou K-C, et al. Synergetic effect of thermal conductive properties of epoxy composites containing functionalized multi-walled carbon nanotubes and aluminum nitride. Composites, Part B. 2012 2012/03/01/;43(2):265-271. doi: https://doi.org/10.1016/j.compositesb.2011.05.027.

174. Yuan F-Y, Zhang H-B, Li X, et al. Synergistic effect of boron nitride flakes and tetrapod-shaped ZnO whiskers on the thermal conductivity of electrically insulating phenol formaldehyde composites. Composites Part A: Applied Science and Manufacturing. 2013 2013/10/01/;53:137-144. doi: https://doi.org/10.1016/j.compositesa.2013.05.012.

175. Zhou T, Wang X, Cheng P, et al. Improving the thermal conductivity of epoxy resin by the addition of a mixture of graphite nanoplatelets and silicon carbide microparticles. Express Polymer Letters. 2013;7:585-594. doi: 10.3144/expresspolymlett.2013.56. English.

176. Yung KC, Liem H. Enhanced thermal conductivity of boron nitride epoxy-matrix composite through multi-modal particle size mixing. J Appl Polym Sci. 2007 2007/12/15;106(6):3587-3591. doi: 10.1002/app.27027.

177. Liem H, Choy HS. Superior thermal conductivity of polymer nanocomposites by using graphene and boron nitride as fillers. Solid State Commun. 2013 2013/06/01/;163:41-45. doi: https://doi.org/10.1016/j.ssc.2013.03.024.

178. Yang K, Gu M. Enhanced thermal conductivity of epoxy nanocomposites filled with hybrid filler system of triethylenetetramine-functionalized multi-walled carbon nanotube/silane-modified nano-sized silicon carbide. Composites Part A: Applied Science and Manufacturing. 2010 2010/02/01/;41(2):215-221. doi: https://doi.org/10.1016/j.compositesa.2009.10.019.

179. Hong J-P, Yoon S-W, Hwang T, et al. High thermal conductivity epoxy composites with bimodal distribution of aluminum nitride and boron nitride fillers. Thermochim Acta. 2012 2012/06/10/;537:70-75. doi: https://doi.org/10.1016/j.tca.2012.03.002.

180. Mulan M, Chaoying W, Tony M. Thermal conductivity of 2D nano-structured graphitic materials and their composites with epoxy resins. 2D Materials. 2017;4(4):042001.

181. Guerra V, Wan C, McNally T. Thermal conductivity of 2D nano-structured boron nitride (BN) and its composites with polymers. Progress in Materials Science. 2019 2019/02/01;100:170-186. doi: https://doi.org/10.1016/j.pmatsci.2018.10.002.

182. Han Z, Fina A. Thermal conductivity of carbon nanotubes and their polymer nanocomposites: A review. Progress in Polymer Science. 2011 2011/07/01;36(7):914-944. doi: https://doi.org/10.1016/j.progpolymsci.2010.11.004.

183. Chen H, Ginzburg VV, Yang J, et al. Thermal conductivity of polymer-based composites: Fundamentals and applications. Progress in Polymer Science. 2016 2016/08/01;59:41-85. doi: https://doi.org/10.1016/j.progpolymsci.2016.03.001.

184. Burger N, Laachachi A, Ferriol M, et al. Review of thermal conductivity in composites: Mechanisms, parameters and theory. Progress in Polymer Science. 2016 2016/10/01;61:1-28. doi: https://doi.org/10.1016/j.progpolymsci.2016.05.001.

185. Chen Q, Dai L, Gao M, et al. Plasma Activation of Carbon Nanotubes for Chemical Modification. The Journal of Physical Chemistry B. 2001 2001/01/01;105(3):618-622. doi: 10.1021/jp003385g.

186. Godbee HW, Ziegler WT. Thermal conductivities of MgO, Al2O3, and ZrO2 powders to 850 C. II. Theoretical. Journal of Applied Physics. 1966;37(1):56-65.

187. Progelhof R, Throne J, Ruetsch R. Methods for predicting the thermal conductivity of composite systems: a review. Polymer Engineering & Science. 1976;16(9):615-625.

188. Hasselman D, Johnson LF. Effective thermal conductivity of composites with interfacial thermal barrier resistance. Journal of Composite Materials. 1987;21(6):508-515.

189. Hamilton R, Crosser O. Thermal conductivity of heterogeneous two-component systems. Industrial & Engineering chemistry fundamentals. 1962;1(3):187-191.

190. Sundstrom DW, Lee YD. Thermal conductivity of polymers filled with particulate solids. Journal of Applied Polymer Science. 1972;16(12):3159-3167.

191. Every AG, Tzou Y, Hasselman DPH, et al. The effect of particle size on the thermal conductivity of ZnS/diamond composites. Acta Metallurgica Et Materialia. 1992;40(1):123-129.

192. Jiajun W, Xiao-Su Y. Effects of interfacial thermal barrier resistance and particle shape and size on the thermal conductivity of AlN/PI composites. Composites Science and Technology. 2004 2004/08/01;64(10):1623-1628. doi: https://doi.org/10.1016/j.compscitech.2003.11.007.

193. Agari Y, Uno T. Estimation on thermal conductivities of filled polymers. Journal of Applied Polymer Science. 1986;32(7):5705-5712.

194. Agari Y, Ueda A, Nagai S. Thermal conductivities of composites in several types of dispersion systems. Journal of Applied Polymer Science. 1991;42(6):1665-1669.

195. Russell H. Principles of heat flow in porous insulators. Journal of the American Ceramic Society. 1935;18(1-12):1-5.

196. Yu W, Xie H, Yin L, et al. Exceptionally high thermal conductivity of thermal grease: Synergistic effects of graphene and alumina. International Journal of Thermal Sciences. 2015;91:76-82.

197. Wang J, Yi XS. Effects of interfacial thermal barrier resistance and particle shape and size on the thermal conductivity of AlN/PI composites. Composites Science & Technology. 2004;64(10–11):1623-1628.

198. Porfiri M, Nguyen NQ, Gupta N. Thermal conductivity of multiphase particulate composite materials. Journal of Materials Science. 2009;44(6):1540-1550.

199. Xue QZ. Model for thermal conductivity of carbon nanotube-based composites. Physica B Condensed Matter. 2005;368(1–4):302-307.

200. Nan CW, Liu G, Lin Y, et al. Interface effect on thermal conductivity of carbon nanotube composites. Applied Physics Letters. 2004;85(16):3549-3551.
201. Shahil KM, Balandin AA. Graphene-multilayer graphene nanocomposites as highly efficient thermal interface materials. Nano Letters. 2012;12(2):861.
202. Shen X, Wang Z, Wu Y, et al. Multilayer Graphene Enables Higher Efficiency in Improving Thermal Conductivities of Graphene/Epoxy Composites. Nano Letters. 2016;16(6):3585.
203. Wang XJ, Zhang LZ, Pei LX. Thermal conductivity augmentation of composite polymer materials with artificially controlled filler shapes. Journal of Applied Polymer Science. 2014;131(8):631-644.
204. Chen L, Sun YY, Xu HF, et al. Analytic modeling for the anisotropic thermal conductivity of polymer composites containing aligned hexagonal boron nitride. Composites Science & Technology. 2016;122:42-49.
205. Chu K, Li WS, Tang FL. Flatness-dependent thermal conductivity of graphene-based composites. Physics Letters Section A General Atomic & Solid State Physics. 2013;377(12):910-914.

Appendix I

Key terms discussed in the review
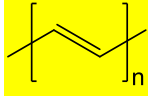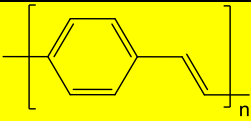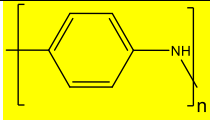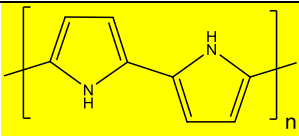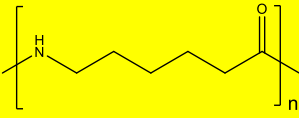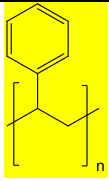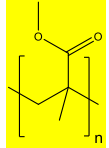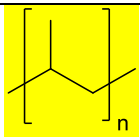
Term	**Definition**
Dispersion	Nature of the filler in the polymer matrix relating to their agglomeration and size and shape distribution.
Multi-functional	In the area of materials or devices, it refers to the fact that the materials can have more than one desirable property, such as thermal conductivity, electrical conductivity, biodegradability, biocompatibility, hence multi-functional.
Thermodynamic reaction control or kinetic reaction control	In the case of polymer nanocomposite processing, the nanoparticles (NP) can be dispersed kinetically by controlling the processing conditions, such as temperature, shearing rate and time, while NP dispersion in one polymer phase or at interfaces is also affected thermodynamically by the surface properties and interfacial interactions.
Surface energy	Surface energy is defined as the energy difference between the bulk of the material and the surface of the material.
Surface chemistry	Surface Chemistry is the study of the phenomena that take place at the surfaces of substances like adsorption, the formation of colloids, heterogeneous catalysis, corrosion, dissolution, crystallization. It is a concept that has widespread applications in industry as well as day-to-day life.
pi-conjugation	A conjugated system has a region of overlapping p-orbitals, bridging interjacent single bonds. They allow a delocalization of π electrons across all the adjacent aligned p-orbitals
Dual Percolation	The formation of two conducting filler networks in a composite
Electron hopping	The movement of electrons through overlapping orbitals, typically along conjugated structures as bridges with the donor, bridge and acceptor energy

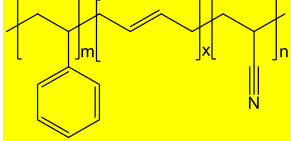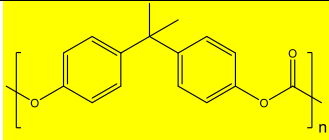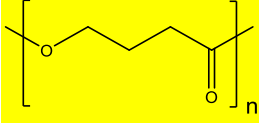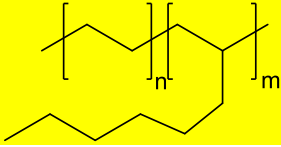|	levels at a similar level.
Electron tunnelling	This is the transport of electrons between a donor and acceptor and can only take place over short ranges – typically less than 5 nm.
Thermal Annealing	The application of temperature and time to alter the polymer morphology
Percolation Threshold	The concentration of filler at which the contact between filler particles forms a conducting network through the matrix
Flexural Strength	The maximum applied stress before a bending failure is observed
Liquid Sensing	The change in response (e.g. electrical resistivity) upon exposure to liquids
Impact Strength	A method of determining the impact resistance of materials. It can be tested by Izod impact test or Charpy Impact test.
Sea-island Morphology	Where one polymer phase is dispersed (islands) and the other polymer phase is continuous (sea)
Dielectric Loss	The dissipation of energy through the movement of charges in an alternating electric field
Dielectric Constant	A measure of the electrical energy storage in a material
Thermal Conductivity	The rate at which heat moves through a material
Thermal Resistance	Measurement describing a materials resistance to heat flow
Phonon	A quasiparticle representing the excited state for the modes of vibrations of elastic structures in interacting particles in quantum mechanics to carry heat
Electromagnetic interference (EMI) and radio frequency interference (RFI)	All electronics emit magnetic and electrical energy, if this energy unintentionally interacts with another device and causes it to malfunction. The EMI shielding efficiency (SE) shows the capacity of the materials to dissipate electromagnetic energy, and is generally expressed in decibels (dB). The specific SE (dB cm2/g) is defined as SE divided by the mass density and thickness, it is a crucial criterion for high-efficiency shielding materials.
Attenuation	Attenuation is one of the principal indicators for measuring the effectiveness of electromagnetic interference shielding. It refers to the difference between an electromagnetic signal's intensity before shielding and its intensity after shielding. Attenuation is marked in decibels (dB) that correspond to the ratio between field strength with and without the presence of a protective medium. The decrease in a signal's intensity, or amplitude, is usually exponential with distance, while the decibel range falls along a logarithmic scale. This means that an attenuation rating of 50 dB indicates a shielding strength ten times that of 40 dB. In general, a shielding range of 10 to 30 dB provides the lowest effective level of shielding, while anything below that range can be considered little or no shielding. Shielding between 60 and 90 dB may be considered a high level of protection, while 90 to 120 dB is exceptional.
volume-exclusion effect	In polymer science, excluded volume refers to the idea that one part of a long chain molecule cannot occupy space that is already occupied by another part of the same molecule.
High stretching sensitivity	The stretching sensitivity indicates the 'resistance- strain dependence' behaviour of stretchable strain sensors. Dynamic strain-sensing test is
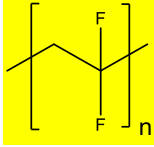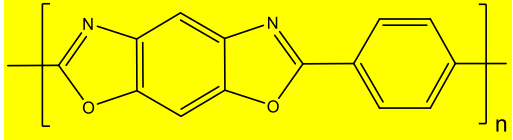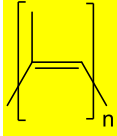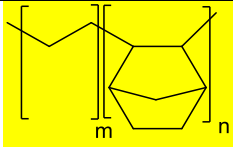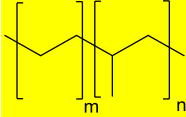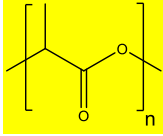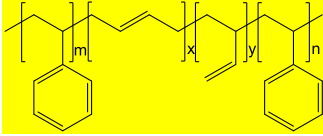
	carried out to evaluate the stability of the strain sensor. Generally successive tensile tests are performed on the materials and the resistance (R) is plotted against time. The sensitivity can be quantitatively characterized by the gauge factor (GF), which is defined as $\Delta R/(\varepsilon R0)$, where ΔR is the change from zero-strain resistance (R0) due to an applied strain. Sensitivity increases with the increase in magnitude of GF.
Mean harmonic approximation	The quasi-harmonic approximation is a phonon-based model of solid-state physics used to describe volume-dependent thermal effects, such as the thermal expansion. It is based on the assumption that the harmonic approximation holds for every value of the lattice constant, which is to be viewed as an adjustable parameter.
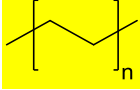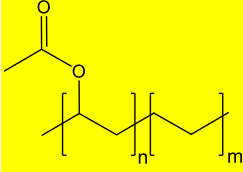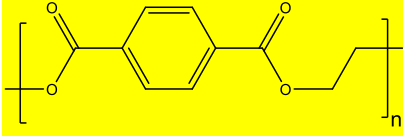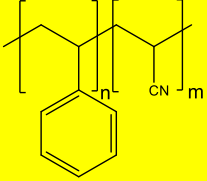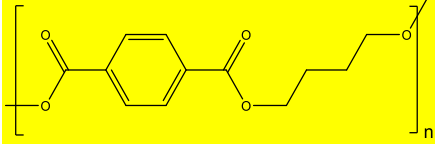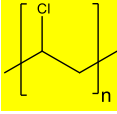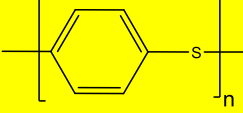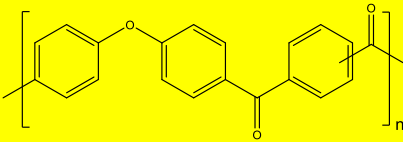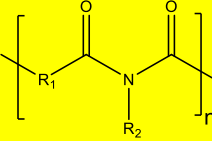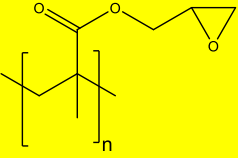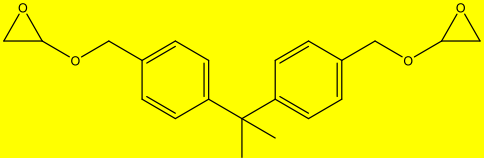
Appendix II

Polymers discussed in the review

Polymer Name	Acronym	Repeat Unit Structure
Polyacetylene	PAc	
Polyphenylene vinylene	PPV	
Polyaniline	PANI	
Polypyrrole	PPy	
Polyamide 6	PA6	
Polystyrene	PS	
Polymethylmethacrylate	PMMA	
Polypropylene	PP	

Polyamide 12	PA12	
Polyvinylidene fluoride	PVDF	
Poly(*p*-phenylene benzobisoxazole	PBO	
Natural Rubber	NR	
Cyclic Olefin Copolymer	COC	
Ethylene Propylene	EP	
Polylactic acid	PLA	
Styrene-butadiene-styrene	SBS	
Acrylonitrile butadiene styrene	ABS	
Polycarbonate	PC	
Poly ε-caprolactone	PCL	
Polyetheylene-co-1-octene	POE	

Polyethylene	PE	
Polyethylene Vinyl Acetate	EVA	
Polyethylene terephthalate	PET	
Styrene Acrylonitrile	SAN	
Polybutylene terephthalate	PBT	
Polyvinyl Chloride	PVC	
Polyphenylene sulphide	PPS	
Polyetherketoneketone	PEKK	
Polyimide	PI	
Polyglycidyl methacrylate	PGMA	
Bisphenol A diglycidyl ether	DGEBA	

Contents